MEASUREMENTS AND ANALYSES OF DECAY RADIOACTIVITY INDUCED IN SIMULATED DEUTERIUM-TRITIUM NEUTRON ENVIRONMENTS FOR FUSION REACTOR STRUCTURAL MATERIALS

BLANKET ENGINEERING

KEYWORDS: *D-T neutrons, radioactivity, experimental validation*

Y. IKEDA *Japan Atomic Energy Research Institute*
Department of Reactor Engineering, Tokai-mura, Naka-gun
Ibaraki-ken 319-11 Japan

A. KUMAR *University of California, Los Angeles*
School of Engineering and Applied Science, Los Angeles, California 90095

C. KONNO, K. KOSAKO, Y. OYAMA, F. MAEKAWA, and H. MAEKAWA
Japan Atomic Energy Research Institute, Department of Reactor Engineering
Tokai-mura, Naka-gun, Ibaraki-ken 319-11 Japan

M. Z. YOUSSEF and M. A. ABDOU *University of California, Los Angeles*
School of Engineering and Applied Science, Los Angeles, California 90095

Received September 29, 1994
Accepted for Publication March 29, 1995

*To meet urgent requirements for data validation, an experimental analysis has been carried out for isotopic radioactivity induced by deuterium-tritium neutron irradiation in structural materials. The primary objective is to examine the adequacy of the activation cross sections implemented in the current activation calculation codes considered for use in fusion reactor nuclear design. Four activation cross-section libraries, namely, JENDL, LIB90, REAC*63, and REAC*175 were investigated in this current analysis. The isotopic induced radioactivity calculations using these four libraries are compared with experimental values obtained in the Japan Atomic Energy Research Institute/U.S. Department of Energy collaborative program on fusion blanket neutronics. The nine materials studied are aluminum, silicon, titanium, vanadium, chromium, MnCu alloy, iron, nickel, niobium, and Type 316 stainless steel. The adequacy of the cross sections is investigated through the calculation to experiment analysis. As a result, most of the discrepancies in the calculations from experiments can be explained by inadequate activation cross sections. In addition, uncertainties due to neutron energy groups and neutron transport calculation are considered. The JENDL library gives the best agreement with experiments, followed by REAC*175, LIB90, and REAC*63, in this order. Clear suggestions for a future direction to improve the overall calculation accuracy are developed based on the current experimental analysis.*

I. INTRODUCTION

Induced radioactivity due to deuterium-tritium (D-T) fusion neutrons is an important issue in terms of reactor safety considerations as well as radioactive waste management of fusion reactors. Extensive efforts have been devoted to radioactivity calculations in various reactor design studies.[1-6] The neutronic design of ongoing projects, e.g., the International Thermonuclear Experimental Reactor (ITER), should address the need

for critical validations of the database relevant to the radioactivity production to meet requirements for licensing. First of all, D-T fusion neutron fields are characterized by the strong 14-MeV neutron peak and low energy flux resulting from the reflected component within the heavily closed geometric configuration of the reactors. Induced radioactivities are characterized by their half-lives, decay modes, and radiation energies. Radioactivities depend on the materials and type of reactions. The neutron spectrum is highly sensitive to the reaction types. Considering all these parameters, thousands of different reactions should be taken into account. The low activation materials consideration is another important factor for waste disposal or recycling of materials.[7-13] It takes a long lead time to develop reasonably low activation materials that meet the requirements for a fusion reactor scenario. However, all of the design calculations assume validity of the current status of knowledge of the activation characteristics in the D-T neutron fields. Many codes and data libraries have been developed in various countries. The quality has been improved by incorporating a wealth of experimental data. An international comparison of these codes has been conducted to realize the appreciable differences in the calculations.[14] Nevertheless, it should noted that these codes and data libraries have not been fully examined by appropriate experiments.[15] To justify the reliability of the database, a more systematic endeavor is requested.

A series of experiments on induced radioactivity have been conducted at the Fusion Neutronics Source (FNS) (Ref. 16) facility in the framework of the Japan Atomic Energy Research Institute/U.S. Department of Energy (JAERI/U.S. DOE) collaborative program on fusion blanket neutronics[17-21] in order to offer the experimental database for the verification of the currently available calculational code system. From the previous preliminary experimental analysis, a lot of serious problems have been pointed out not only in the activation cross-section libraries implemented in various calculation code systems,[22-25] but also in decay data libraries, even for the materials used in the major structural components.[26-32]

This paper focuses on demonstrating the way to validate the calculation code system. First, a brief outline of the experiments and an analysis are presented. Second, the uncertainty range in all parameters pertinent to decay radioactivity production is discussed based on calculation to experiment (C/E) analysis. This paper deals with several recent activation cross-section libraries, including the JENDL activation file[33] and two versions of data libraries in REAC*3 (Ref. 34). The activation file, CROSSLIB90, which is implemented in the THIDA code system,[23] was also investigated.

II. OUTLINE OF THE EXPERIMENT

II.A. Strategy

The strategy for these induced radioactivity experiments is shown in Fig. 1. The experiments primarily

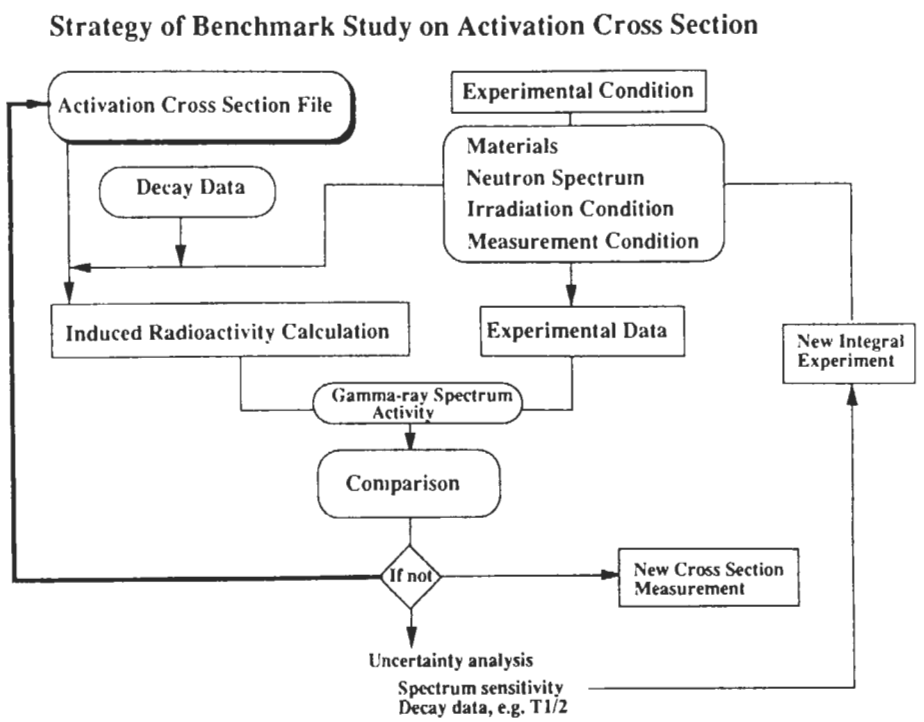

Fig. 1. Flow of validation for induced radioactivity calculation.

were designed for benchmarking the code and data. Induced radioactivity, I_{act}, is given as

$$I_{act} = M \cdot D_i \cdot T_i(t) \int_{E_{min}}^{E_{max}} \sigma(E)_i \cdot \Phi(E) \cdot dE \ , \qquad (1)$$

where

M = parameters associated with materials irradiated

D_i = decay properties for i'th radioactivity

$T_i(t)$ = time-related parameter for i'th radioactivity

$\sigma(E)$ = activation cross section for the i'th radioactivity production

$F(E)$ = neutron flux spectrum.

It should be noted that I_{act} is formed with multiple factors. When the $\sigma(E)$ is investigated, the most important factor is the neutron environment selection because simulation of the fusion neutron field is directly reflected in the validity of the benchmark. Effectiveness of the study strongly depends on the availability of the neutron fields. We have chosen two neutron spectrum fields in the experimental system configuration of Phase-IIC of the JAERI/U.S. DOE collaborative program on Fusion Neutronics.[17,18,35,36] Since the details of the experimental configuration have been described previously,[26–30,35] an outline of experiments is reviewed here focusing on the neutron field characteristics and activity measurement. As the measured quantity to be compared with calculations, the decay rate of isotopic radioactivity was selected for this benchmark study. Materials, highlighted here, were elements for structural components.

II.B. Neutron Spectrum

The cross-sectional view of the experimental system of the Phase-IIC is given in Fig. 2. The positions of sample materials are indicated by A and B, at 100 mm from the D-T source and at 820 mm from the source corresponding to a 50-mm depth into the Li_2O region. A rotating neutron target system was employed to produce high-intensity D-T neutrons. The experimental system consisted of (a) the Li_2O solid breeder zone in which three polyethylene layers were imbedded to simulate the water coolant, (b) the Li_2CO_3 enclosure, and (c) the polyethylene insulator zone in the outermost region. The D-T neutron source was located inside the cavity. This configuration was considered to be the best choice to realize the D-T fusion neutron environment with reflecting component. It was accepted that the position of A corresponded to the locations near the first wall. On the other hand, the position B was considered to be a representative one in the breeder's blanket zone with certain amounts of the lithium element.

Figure 3 shows the neutron spectra of A and B, calculated by MORSE-DD (Ref. 37) with FUSION-J3 (Ref. 38) based on the JENDL-3 nuclear data library.[39] Spectrum A represents a neutron spectrum at locations near the first wall where the 14-MeV neutron flux dominates the field. Spectrum B is characterized by a reduced 14-MeV neutron flux, due to a larger distance from the D-T neutron target, attenuation in the Li_2O region, and relatively high neutron flux in about the MeV region. However, thermal neutron flux is lower than that in A because of the large absorption cross section of the $^6Li(n,t)^4He$ reaction in Li_2O, where the samples were irradiated. The digital data of fluxes were given in a previous report.[40]

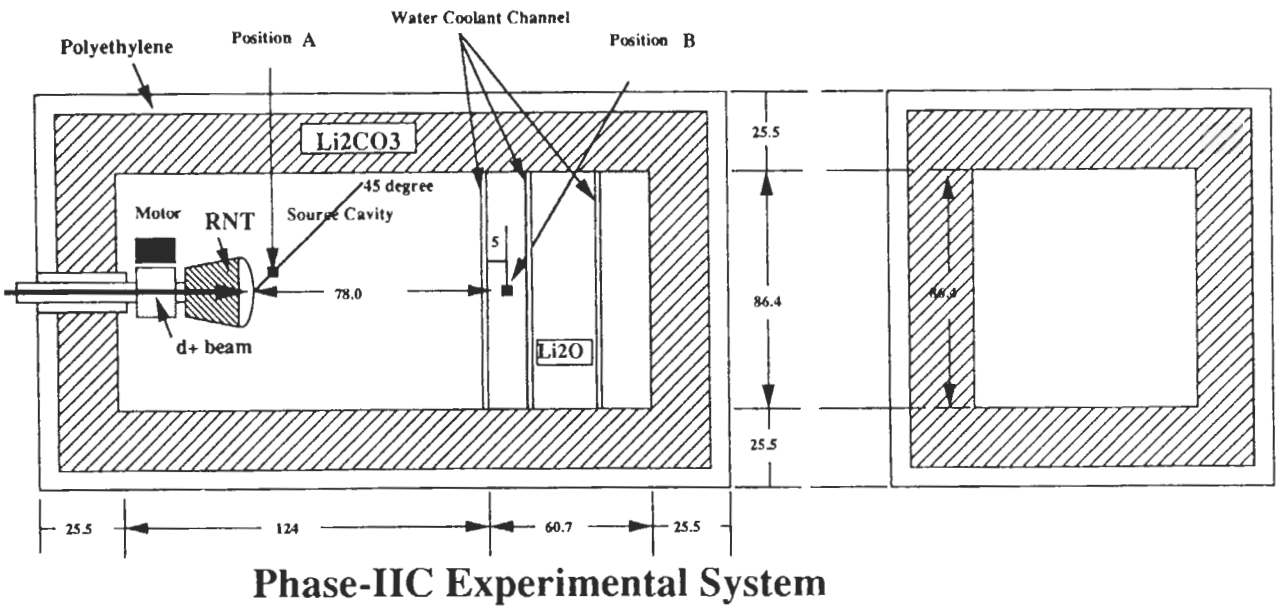

Fig. 2. Cross-sectional view of the Phase-IIC experimental system.

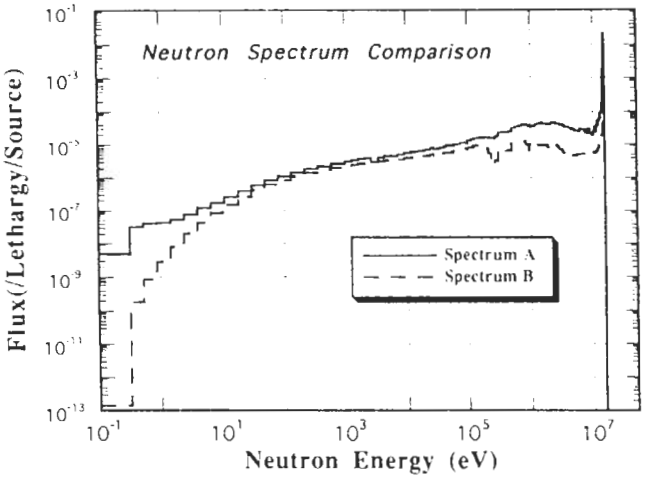

Fig. 3. Neutron spectra at positions A and B, calculated with MORSE-DD incorporated with JENDL-3.

II.C. Materials

This paper deals with candidate materials for fusion structural components. Table I gives the basic data for sample materials investigated. Aluminum and silicon are the major components for the aluminum alloy and SiC for the low activation materials. Titanium, vanadium and chromium are the major constituents of the vanadium alloy (V–5 Cr–5 Ti) addressed in a comprehensive ITER design. Iron, nickel, again chromium, and manganese are the elements common in austenite steels, e.g., Type 316 stainless steel. The importance of cobalt is recognized as an impurity in almost all material, which produces long-lived ^{60}Co. Copper is also a major material used in many parts of the device. Other materials for plasma-facing and functional elements are treated in a companion paper.[41]

II.D. Irradiation and Counting Schedule

The D-T neutrons were generated by bombarding a Ti-^{3}T target with deuteron beams, the energy and intensity of which were 350 keV and 20 mA, respectively. The nominal D-T neutron yield for sample irradiations was $\sim 1.2 \times 10^{12}$ n/s at the neutron source. Two irradiation schemes of "short" for 30 min and "long" for 10 h were applied for both A and B sample positions. Induced radioactivities were measured at various cooling times after irradiation, which ranged from 10 min to several hours for short, and from 1 h to several days for long.

II.E. Induced Radioactivity Measurement

Emission rates of gamma rays, which are associated with specific radionuclides of interest, are used as the experimental values to be compared with calculations. The gamma-ray spectrum is also directly compared with calculations based on the same library of JENDL. Both comparisons give absolute validation of the calculation that is a product of neutron flux, activation cross section, and decay properties, i.e., half-life and gamma-ray emission probability.

TABLE I

Atomic Weight, Density, and Chemical Composition of Primary Impurities in the Samples Used in Induced Activity Irradiations

Sample Material	Atomic Weight (g)	Density (g/cm^3)	Chemical Composition (wt%)
Aluminum (Al)	26.98154	2.70	Al (99.97), Mg (0.006)
Silicon (Si)	28.0855	2.42	Si (99.99)
Titanium (Ti)	47.88	4.5	Ti (99.6), O (0.13), Al (0.03), Cr (0.03), Mn (0.03), Ni (0.03), V (0.03), Fe (0.02)
Vanadium (V)	50.9415	5.87	V (99.82), Si (0.044), Ta (0.03), O (0.03), Mo (0.013), Zr (0.01), Fe (0.01), Al (0.01), Hf (0.01)
Chromium (Cr)	51.996	7.14	Cr (99.0), Fe (0.43), Al (0.10), Si (0.05)
Iron (Fe)			Fe (99.92), Mn (0.059), C (0.02)
Mn-Cu alloy (MnCu)	---	7.58	Mn (79.78), Cu (19.66), Ni (0.46), Fe (0.07)
Iron (Fe)	55.847	7.86	Fe (99.92), Mn (0.059), C (0.02)
Cobalt (Co)	58.9332	8.71	Co (99.95), Ni (0.04)
Nickel (Ni)	58.69	8.80	Ni (99.97), C (0.016)
Type 316 stainless steel	---	7.90	Fe (66.22), Cr (17.75), Ni (11.60), Mo (2.08), Mn (1.33), Si (0.42), Co (0.19), Cu (0.34), V (0.06)
Niobium (Nb)	92.9064	8.57	Nb (99.91), Ta (0.018), Zr (0.01)

Radioactivity decay rate, DR, is defined as,

$$DR = \frac{\lambda \cdot C}{\epsilon \cdot w \cdot \mu \cdot S_f \cdot Y_n \cdot [1 - \exp(-\lambda \cdot t_m)]} , \quad (2)$$

where

λ = decay constant of the specific radioactivity

C = measured gamma-ray counts

ϵ = detector efficiency

w = sample weight

μ = gamma-ray self-absorption coefficient

S_f = correction factor for the radioactivity saturation during the irradiation

Y_n = source neutron strength

t_m = collection time for the activity measurement.

The DR was assigned to be the quantity for the experimental analysis. To deduce the DR at a cooling time, the strongest gamma-ray line, identified to a specific radionuclide decay, was used along with other necessary experimental conditions given in Eq. (2). In addition, the measured gamma-ray spectrum was directly compared with calculation. This spectrum comparison provides a measure for overall adequacy of the calculation system because the spectrum includes a decay profile during the counting.

III. EXPERIMENTAL ANALYSIS

III.A. Calculation Codes and Nuclear Data Libraries

The activation cross-section libraries, examined here, were (a) a multigroup activation cross-section library with 125-energy group structure based on the JENDL activation file,[33] which is now under testing in the working group of one of the Japanese Nuclear Data Committees, (b) CLOSSLIB90 with 42 energy groups, which was implemented in the induced radioactivity calculation code system, THIDA (Ref. 23), (c) a cross-section data file with 63 multigroups in REAC*3 (Ref. 34) code system, and (d) an updated cross-section library with 175 multigroups (VITAMIN-J format) for the REAC*3 code system. Table II summarizes the codes and libraries used in this experimental analysis. Code ACT4, the main module for activity calculation in the THIDA code system, was employed for two libraries of (a) and (b). The main module of REAC was used for both calculations with two versions of the REAC*3 libraries. Gamma-ray decay data and chain libraries were created generally based on ENSDF (the Evaluated Nuclear Structure Data File available at Brookhaven National Laboratory). The decay and chain libraries implemented in the THIDA code system were used for the calculation with CROSSLIB90. In general, there is no serious discrepancy among decay libraries. Thus, through the comparison of radioactivity calculations with experimental measurement, straightforward discussion on the cross-section validity is possible.

III.B. Neutron Spectrum Condition

As noted before, validity of the neutron spectrum is of fundamental concern for the integral test of induced radioactivity calculation. The neutron spectra at positions of A and B, calculated with MORSE-DD (Ref. 37), were collapsed into energy groups corresponding to multigroup cross-section libraries, i.e., 42 for CROSSLIB90, 63 for REAC*3 old, and 175 for REAC*3 new. The original neutron spectra with 125 energy groups were directly used for the JENDL calculation. The comparison of these collapsed neutron spectra at position A is given in Fig. 4. The discrepancies among the integrated flux over 10 MeV agreed within $\pm 0.01\%$ with each other. It should be noted that there is a large difference in the energy boundaries among the libraries. The coarse energy bin in the 63-energy-groups structure and in the 42-energy-group structure shows a poor resolution near the D-T neutron peak. As indicated by the 125-energy-group structure, there is a distribution in the neutron flux around the D-T neutron peak. The neutron flux of the 175-group-structure almost follows the flux structure of the 125 energy groups.

TABLE II

Induced Radioactivity Calculation Codes and Data Libraries

Code Systems	Activation Files	Neutron Groups	Decay Data Libraries
ACT4[a]	JENDL Activation File	125	ENSDF γ-56
ACT4	CROSSLIB90[b]	42	GAMMLIB[c] γ-56
REAC*3	REAC*3 old	63	ENSDF γ-22
REAC*3	REAC*3 new	175[d]	ENSDF γ-22

[a]Main module for induced radioactivity calculation in the THIDA code system.
[b]Activation cross-section data library in the THIDA code system.
[c]Decay gamma-ray data library in the THIDA code system based on the Table of Isotopes.
[d]VITAMIN-J format.

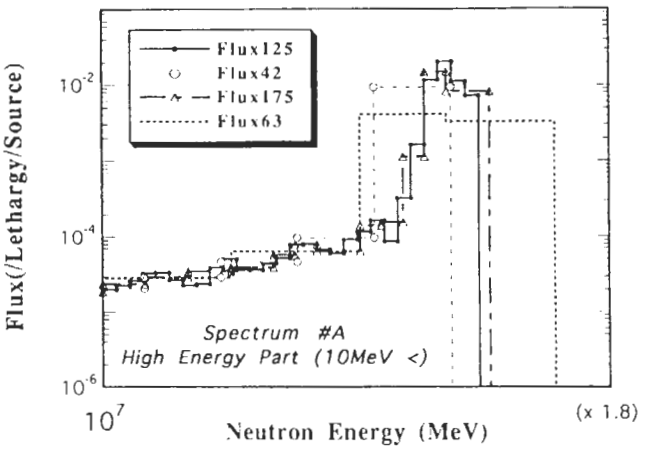

Fig. 4. Comparison of neutron energy spectra with different energy groups around a D-T neutron peak region.

III.C. Comparison of Calculations with Experiments

The gamma-ray emission rates corresponding to observed radionuclides were derived from the induced radioactivity calculations. The emission rate was calculated as per source neutron and per unit weight to be compared with the experimental data given in Eq. (2) in Sec. II.E. The discussion is based on the C/E ratio.

IV. RESULTS

The results of experimental analysis are given for materials and isotopic radionuclide products. The calculations with libraries of the JENDL activation file, the CROSSLIB90, the REAC library with 63 energy groups, and the REAC library with 175 energy groups, are, hereafter, denoted as JENDL, LIB90, REAC*63, and REAC*175, respectively. The indices for irradiation and cooling times are assumed the same as described in the experiments. The C/Es are summarized in Table III. The C/Es of importance are illustrated in the figures. The cross-section curves for important reactions are also illustrated in figures comparing the values in the different libraries.

IV.A. Aluminium

Figure 5 shows the C/Es for ^{27}Mg and ^{24}Na decay rates in both aluminum samples at positions A and B.

IV.A.1. ^{27}Mg

The activity of ^{27}Mg is produced via the ^{27}Al$(n,p)^{27}$Mg reaction, which is well known in dosimetry application. The cross section has been extensively studied.[42] As the four libraries give similar cross-section values in the 14-MeV region, all calculations exhibited close C/Es, although there are slight underestimations ranging from 0.85 to 0.95. Though these C/Es seem adequate from consideration of the overall experimental uncertainty range of ±10%, cross sections should be reevaluated. Recent precise measurements for this cross section[42] suggest that the data in an energy region from 14.5 to 15 MeV in JENDL are 5 to 10% lower than the new experimental data for this reaction.

IV.A.2. ^{24}Na

The reaction of ^{27}Al$(n,\alpha)^{24}$Na is one of most accurately studied, and the cross section has been evaluated precisely. The JENDL gives most preferable results with C/Es around 1.0. The REAC*63 shows similar good results. The LIB90 is slightly larger than 1.0 by 10%. The cross section of REAC*175 is very close to those of JENDL and REAC*63, as shown in Fig. 6. However, C/E with REAC*175 is systematically high being 1.3 to 1.4 for all cases. These overestimations are due to contribution of ^{27}Al$(n,\alpha)^{24m}$Na, the cross-section curve of which is shown in Fig. 6. The ^{24m}Na is the isomeric state of ^{24}Na and deexcites to the ground state of ^{24}Na with a 2-ms half-life. In the REAC*175, both the reactions are treated separately. However, in general, the cross section of ^{27}Al$(n,\alpha)^{24}$Na is given as a sum of both the metastable and ground state productions. In this view, the cross section of ^{27}Al$(n,\alpha)^{24m}$Na is doubly counted in the REAC*175 library. For completeness, different reaction paths should be treated independently as in the REAC*175. However, the cross section for the metastable state production should be subtracted from the ground-stated production cross section.

The good results of ^{24}Na except for the case of REAC*175, demonstrate that the neutron spectra used in this analysis are adequately validated as far as the high energy fluxes are concerned. This assures the validity of this test for many threshold reactions.

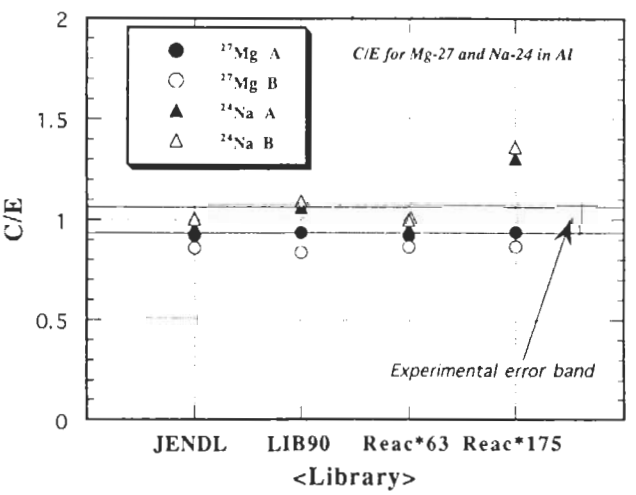

Fig. 5. The C/E values of isotopic radioactivities in aluminum.

TABLE III

Summary of C/E

Element	Nuclide	ID	JENDL	LIB90	REAC*63	REAC*175
Aluminum	^{27}Mg	A	0.92	0.94	0.92	0.94
		B	0.86	0.84	0.87	0.87
	^{24}Na	A	1.05	1.16	1.05	1.42
		B	1.01	1.09	1.00	1.36
Silicon	^{28}Al	A	1.00[a]	1.41	4.35	4.40
	^{27}Mg	A	0.92	0.70	7.00	7.52
	^{29}Al	A	0.83	0.41	1.84	0.93
Titanium	^{45}Ti[b]	A	1.15	0.75	1.95	1.79
		B	1.12	0.65	1.49	1.38
	^{46}Sc	A	1.14	1.11	1.13	1.13
	^{47}Sc	A	1.09	0.79	2.61	1.36
		B	1.12	0.88	2.32	1.48
	^{48}Sc	A	1.20	1.20	1.16	1.31
		B	0.99	0.99	0.98	1.10
Vanadium	^{48}Sc	A	1.04	0.99	1.32	1.10
		B	1.08	1.03	1.32	1.11
	^{51}Ti	A	0.54	0.58	0.77	0.69
		B	0.61	0.64	0.83	0.74
	^{52}V	A	[c]	0.88	1.01	1.01
		B	[c]	1.73	1.51	1.51
	^{47}Sc	A	1.00[a]	1.00	1.67	1.34
		B	1.00[a]	1.11	15.1	13.6
Chromium	^{51}Cr	A	1.05	0.89	1.08	1.07
		B	0.97	0.90	1.04	1.04
	^{49}Cr	A	1.27	0.64	2.55	1.76
Manganese	^{56}Mn	A	1.22	1.24	1.47	1.21
		B	1.57	1.53	1.90	1.51
	^{54}Mn	A	1.01	0.96	0.97	1.04
		B	0.96	0.92	0.92	0.99
	^{52}V	A	1.06	1.06	1.26	1.17
Iron	^{56}Mn	A	1.02	1.09	0.93	0.95
		B	1.05	1.08	1.01	1.03
	^{54}Mn	A	0.96	1.12	0.97	0.94
	^{51}Cr	A	1.00	1.00	0.83	1.01
Cobalt	$^{58m+g}$Co	A	1.39	1.04	2.32	1.16
		B	1.30	1.01	2.21	1.12
	^{56}Mn	A	1.00	1.06	0.88	0.92
		B	1.11	1.11	1.00	1.03
Cobalt	^{59}Fe	A	0.75	0.75	0.94	1.11
		B	0.85	0.85	1.02	1.18
	$^{60m+g}$Co	B	1.86	3.33	4.68	2.60
Nickel	^{57}Ni	A	1.05	0.87	1.00	0.97
		B	1.05	0.79	0.83	1.11
	^{57}Co	A	0.92	0.86	1.14	0.88
		B	1.06	1.00	1.27	0.99
	$^{58m+g}$Co	A	1.07	1.92	2.09	1.08
		B	1.07	1.46	1.72	1.26
	$^{60m+g}$Co	A	0.71	1.19	1.29	0.78
	^{62m}Co	A	4.97	1.38	2.79	1.85

(Continued)

TABLE III (Continued)

Element	Nuclide	ID	JENDL	LIB90	REAC*63	REAC*175
Copper	$^{62}Cu^{b}$	A	1.06	0.98	1.18	1.36
		B	1.12	1.06	1.23	1.41
	$^{64}Cu^{b}$	A	1.26	1.25	1.23	1.25
		B	1.04	0.81	0.76	0.82
	^{65}Ni	A	1.75	1.78	1.52	1.52
	^{62m}Co	A	0.18	1.72	1.38	0.48
Type 316 stainless steel	^{56}Mn	A	0.93	0.99	0.80	0.84
		B	0.87	0.89	0.70	0.71
	^{54}Mn	A	0.71	0.76	0.43	0.42
		B	0.87	0.90	0.64	0.63
	^{57}Ni	A	1.10	0.94	1.06	1.06
		B	1.12	1.07	1.12	1.12
	$^{58m+g}Co$	A	0.93	1.61	1.75	1.08
		B	1.15	1.57	1.86	1.35
	^{57}Co	A	0.71	0.66	0.99	0.76
		B	1.05	0.99	1.45	1.11
	^{49}Cr	A	0.78	0.18	1.72	1.19
	^{51}Cr	A	0.65	0.57	0.72	0.72
		B	0.67	0.61	0.73	0.74
	^{99}Mo	A	0.82	0.87	0.68	0.77
		B	1.33	1.40	1.11	1.51
Niobium	^{90m}Y	A	0.72	0.65	1.27	0.71
		B	0.82	0.73	1.23	0.73
	^{92m}Nb	A	1.10	1.04	1.12	1.20
		B	1.04	0.99	1.11	1.13

[a]Relative to JENDL (no experimental data were observed).
[b]Data were deduced from annihilation gamma ray.
[c]No corresponding reaction in the library.

IV.A.3. ^{26}Al

This is one of the important radionuclides for long-lived waste considerations due to an extremely long half-life of 7.2×10^5 yr. As there is no experimental data due to limitation of detection of such a small decay rate, it is worthwhile to compare the cross sections in the libraries investigated. Ratios of calculated radioactivities to that with JENDL were examined knowing that the cross section of JENDL is consistent with recent experimental data for this reaction cross section.[43] The small ratio of 0.3 in LIB90 compared to JENDL corresponds to a lower cross section of LIB90 than that of JENDL for a 14-MeV neutron. High ratios for REAC*63 and REAC*175 compared to JENDL are attributable to large cross-section values at the 14-MeV region in both libraries. More specific analysis focusing on the long-lived radioactivity is separately treated in a companion paper to be issued.

IV.B. Silicon

As all activities in silicon are short-lived, only one case is available for the analysis. The C/Es for ^{27}Mg and ^{29}Al are shown in Fig. 7.

IV.B.1. ^{27}Mg

The reaction of $^{30}Si(n,\alpha)^{27}Mg$ is expected to be a major contributor in the production of ^{27}Mg from silicon. The JENDL gives reasonable agreement with the experiment. The LIB90 underestimates the measurements by 30%. This reflects a lower cross section at 14 MeV than that of JENDL. On the other hand, REAC*63 and REAC*175 considerably overestimate the measurement values by factors of 7 and 7.5, respectively. In the libraries of REAC*63 and REAC*175, rare reactions of $^{28}Si(n,2p)$, $^{30}Si(n,n'^{3}He)$ and $^{29}Si(n,^{3}He)$ are included, which produce ^{27}Mg. However, the cross sections for these rare reactions shown in Fig. 8a seem unreasonably large, by two to three orders of magnitude from reaction systematic considerations and reaction Q-values. In particular, the reaction of $^{28}Si(n,2p)$ has large impact on the ^{27}Mg production because of 92.18% of abundance of ^{28}Si, while ^{30}Si has only 3.12% abundance in silicon. In general, these rare reaction cross sections have not been measured experimentally and values in the libraries are based on some theoretical model calculations. This example demonstrates the importance of validation of the database through experimental analysis.

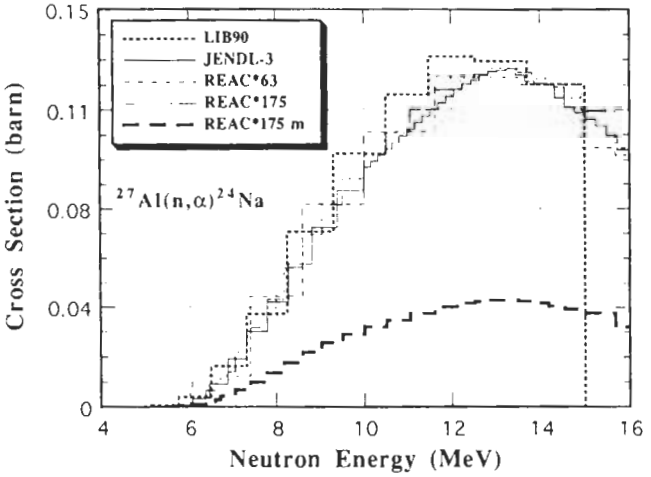

Fig. 6. Cross sections for the $^{27}Al(n,\alpha)^{24}Na$ in the four different libraries.

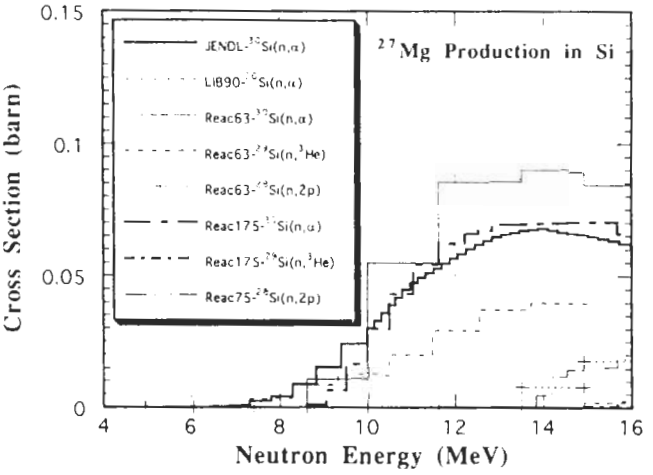

Fig. 8a. Cross sections for ^{27}Mg production in silicon in the four different libraries.

IV.B.2. ^{29}Al

REAC*175 gives the best agreement with measurement. Though JENDL slightly underestimated the experimental results, it is within the experimental uncertainty. The considerably large underestimation and overestimation in LIB90 and REAC*63 are due to small and high cross-section values for $^{29}Si(n,p)^{29}Al$ at the 14-MeV energy region in these two libraries, respectively. The contribution of $^{30}Si(n,np)$ could not be overlooked because of a comparable constituent of ^{30}Si to ^{29}Si in silicon. The better agreement in REAC*175 shows that the $^{30}Si(n,np)$ cross section in the REAC*175 library is properly given, while that in JENDL seems too small.

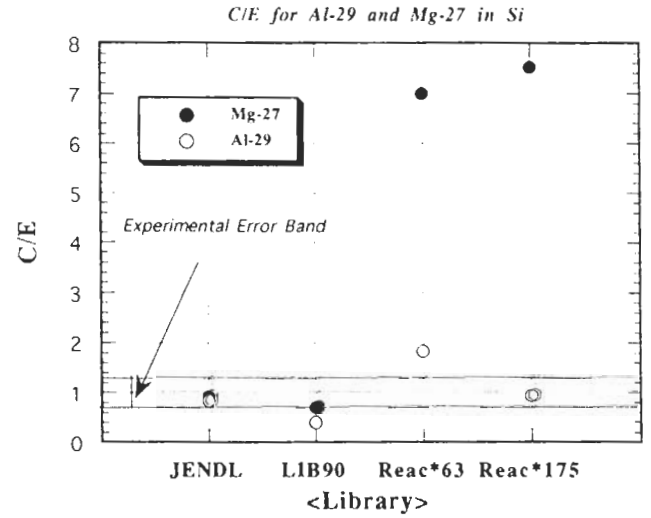

Fig. 7. C/E values of isotopic radioactivities in silicon.

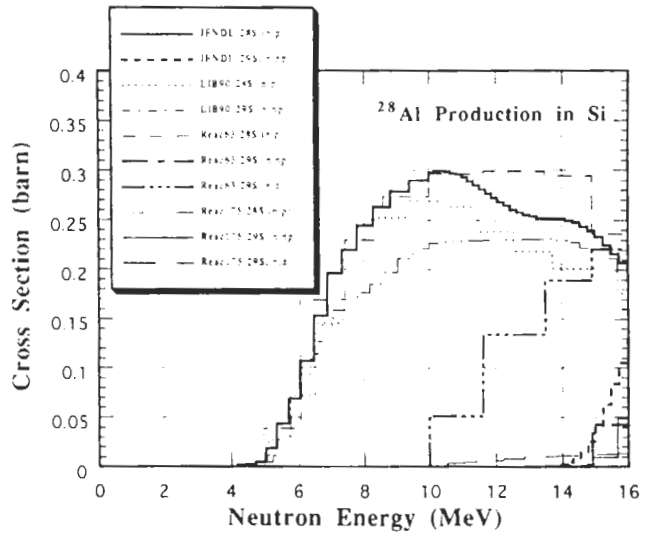

Fig. 8b. Cross sections for ^{28}Al production in silicon in the four different libraries.

IV.B.3. ^{28}Al

No gamma ray was observed because of the short half-life of 2.24 min. The LIB90 exhibits a 40% high ratio. Both REAC*63 and REAC*175 give large values by a factor of 4.4. This large value could not be explained by the cross-section differences in the $^{28}Si(n,p)$ reaction, which is the major contributor to ^{28}Al production. As shown in Fig. 8b, the cross section of $^{29}Si(n,d)$ in REAC*63 seems too large for (n,d) and (n,np) reaction cross sections. Furthermore, the abundance of ^{29}Si is only 3% in silicon, so that the contribution of $^{29}Si(n,np)$ and (n,d) is small. The ^{28}Si is the daughter of ^{28}Mg, which has a long half-life of 21 h. If ^{28}Mg is produced in silicon, this is another path to ^{28}Si, which

gives a slow decay curve at a long cooling time. Actually, at the end of the irradiation, JENDL, REAC*63, and REAC*175 gave close decay rates of ^{28}Al. However at the cooling time of about 37 min, REAC*63 and REAC*175 give a 4 times larger value than JENDL. In the cross section libraries of REAC*63 and REAC*175, the reaction of ^{29}Si$(n,2p)$ is installed to produce ^{28}Mg, with a considerably large cross section of 7 mb at the 14-MeV energy range. After 37 min cooling, the activity level of ^{28}Al become 10^{-5} of the initial. This means that ^{28}Mg production, which is $\frac{1}{30}$ in abundance and $\frac{1}{30}$ in cross section dominates the ^{28}Al activity at the time of concern. In conclusion, the cross section of 7 mb seems unreasonably overestimated by two to three orders of magnitude in the REAC libraries.

IV.C. Titanium

IV.C.1. ^{45}Ti

The β^+-emitter, ^{45}Ti ($T_{1/2}$ = 3.09 h), is produced via the ^{46}Ti$(n,2n)^{45}$Ti reaction. The C/E trends with libraries shown in Fig. 9 correspond to the difference in the cross sections at 14 MeV. However, the scattered nature in the C/Es for the different measurement runs are observed, and they are not systematic with the spectrum changes. One possible explanation to be addressed is the inconsistency in experimental values due to the 511-keV annihilation gamma-ray counts. Because of β^+ distribution around the titanium sample, which was placed at a position close to the detector, detector efficiency may change considerably the lower counting rate. The correction for the counting loss seemed to be insufficient. The data for spectrum B measured at the standard detection position has less effect of this correction. The JENDL slightly overestimated the experiment by 12%; LIB90 underestimated by more than 30%; REAC*63 overestimated by 23%; and REAC*175 overestimated by 14%. These differences in C/Es are explained by the differences in the cross sections around 14 MeV.

IV.C.2. ^{46}Sc

The ^{46}Sc activity is produced via both the ^{46}Ti(n,p) and ^{47}Ti(n,np) reactions. Considering comparable abundances of ^{46}Ti and ^{47}Ti, the ^{47}Ti(n,np) reaction contributes ~30% of ^{46}Sc production as far as the 14-MeV neutron flux is concerned. All libraries give almost the same C/E values for all runs. From the cross sections shown in Fig. 10a, however, REAC*175 gives a lower production rate by 30%. The cross section for ^{46}Ti$(n,p)^{46}$Sc in REAC*175 is systematically lower than those in the other libraries, where values at 14 MeV

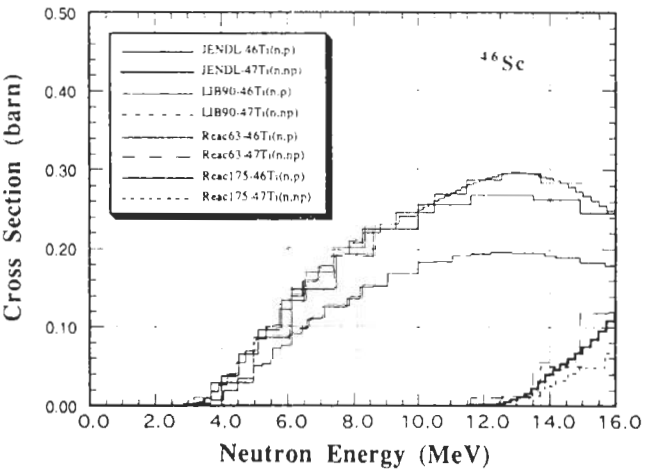

Fig. 10a. Cross sections for ^{46}Sc production in titanium in the four different libraries.

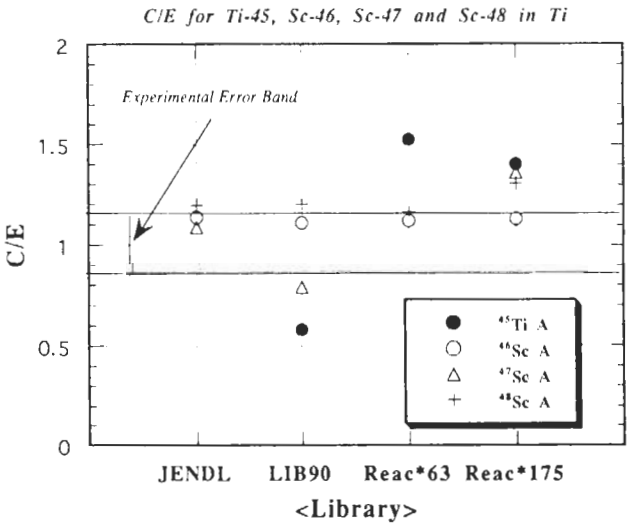

Fig. 9. The C/E values of isotopic radioactivities in titanium.

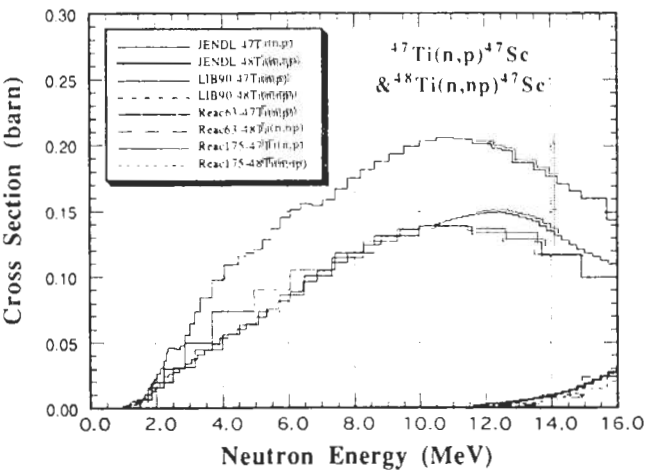

Fig. 10b. Cross sections for ^{47}Sc production in titanium in the four different libraries.

are consistent with the recent experimental values. The similar C/E in REAC*175 to those of other libraries is attributable to additional contributions to ^{46}Sc production by the reactions of ^{48}Ti$(n,t)^{46}$Sc (0.1 mb) and the metastable state ($T_{1/2}$ = 18.7 s) production reactions via ^{47}Ti$(n,np)^{46m}$Sc (30 mb) + ^{47}Ti$(n,d)^{46m}$Sc (3 mb), which are included in the REAC*175 library. Note that the cross-section values given in parentheses are values at 14 MeV. These additional contributions, compensated for the low primary production cross section indicated earlier. The other libraries adequately predicted ^{46}Sc within the experimental uncertainty of ±15%.

IV.C.3. ^{47}Sc

The ^{47}Sc is produced via not only the ^{47}Ti(n,p) reaction but also the ^{48}Ti(n,np) + (n,d) reactions in titanium. Because of the ten times higher abundance of ^{48}Ti than that of ^{47}Ti, the contribution from the ^{48}Ti(n,np) reaction is expected to be comparable to ^{47}Ti(n,p) even though the cross section at 14 MeV is ten times lower than that of the ^{47}Ti(n,p) reaction. The C/Es of JENDL and LIB90 as shown in Fig. 9 are in the reasonable range of the experimental uncertainty. The overestimation in REAC*175 by 40 to 50%, however, is reflected by the large cross section of the ^{47}Ti$(n,p)^{46}$Sc reaction as shown in Fig. 10b. The REAC*63, as shown in Fig. 9, largely overestimated the measurements by a factor of 2.3 to 3.0. This large overestimation could not be explained from the cross-section curves of the contributing reactions mentioned earlier. It was found that the cross section of ^{48}Ti(n,d) is unreasonably large being 50 mb at 14 MeV in the REAC*63 library. One order of magnitude of higher abundance of ^{48}Ti enhanced the contribution of ^{47}Sc production unreasonably in REAC*63.

IV.C.4. ^{48}Sc

There is an inconsistency in the C/E for ^{48}Sc production in terms of different runs as shown in Fig. 9. As the main contribution for ^{48}Sc comes from ^{48}Ti$(n,p)^{48}$Sc, the contributions of ^{49}Ti$(n,np)^{48}$Sc and ^{50}Ti$(n,t)^{48}$Sc are expected to be small because of the small cross sections and small abundances of ^{49}Ti (5.46%) and ^{50}Ti (5.25%) relative to ^{48}Ti (73.99%) in titanium. The overestimation by 60 to 80% for case A in all libraries should be attributed to the inadequacy in the experimental value; strong counting losses due to the coincidence sum effect for ^{48}Sc gamma rays occurs when the sample-to-detector distance is short because of the cascade decay of three gamma-ray lines in the decay of ^{48}Sc. This correction was largely insufficient in this case. The systematic overestimations for cases A and B are also attributable to the insufficient correction of this coincidence sum effect. Revised data using a directly measured counting loss correction gives reasonable agreement with calculations, being close to 1.0. The range of slight overestimation in the REAC*175 calculation corresponds to higher cross sections of the ^{48}Ti(n,p) reaction than those in the other libraries.

IV.D. Vanadium

The importance of vanadium in the consideration of vanadium alloy for major structural material with low-activation residual is stressed in recent ITER reactor designs in order to meet radiation regulation. Along with titanium and chromium, the activation database in vanadium should be investigated and thoroughly validated. The C/Es for major activities are shown in Fig. 11.

IV.D.1. ^{48}Sc

This activity is produced predominantly via the reaction of ^{51}V$(n,\alpha)^{48}$Sc. The C/Es of JENDL, LIB90, and REAC*175 are in a reasonable range from 0.9 to 1.1, while REAC*63 overestimated the measurement by ~30%. This is simply because the cross section at 14 MeV in REAC*63 is higher by 30% than those in the other libraries.

IV.D.2. ^{51}Ti

All calculations underestimated the measurement with the C/Es ranging from 0.62 to 0.83. The cross sections of ^{51}V$(n,p)^{51}$Ti ($T_{1/2}$ = 5.8 min) in all libraries are in good agreement with recent experimental values.[16] A possible reason for this underestimation is because the experimental values were improperly large. It is strongly recommended to do an irradiation experiment focusing on the short-lived activity production. Nevertheless, this range of discrepancy does not yield a serious problem with induced radioactivity predictions in

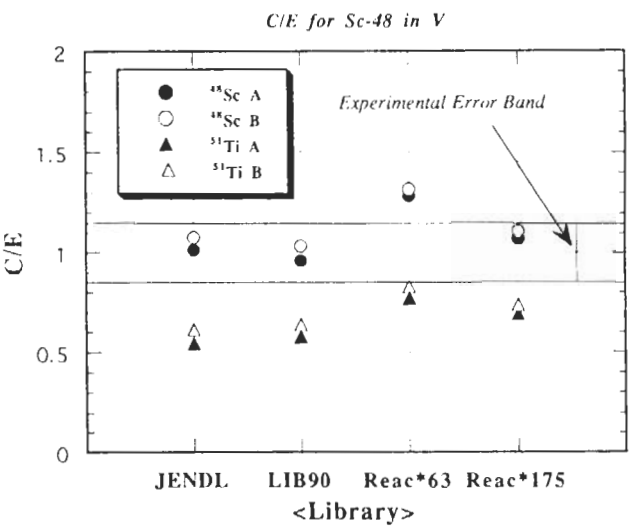

Fig. 11. The C/E values of isotopic radioactivities in vanadium.

fusion reactor operations due to the short-lived characteristics of vanadium.

IV.D.3. ^{52}V

The reaction of $^{51}V(n,\gamma)^{52}V$ ($T_{1/2}$ = 3.76 min) is the major source of ^{52}V production. Unfortunately, JENDL doesn't include this reaction cross section. Although the C/Es for spectrum A are in a reasonable range in all calculations, the C/Es for spectrum B are >1.5. This discrepancy should be investigated from spectrum sensitivity to (n,γ) reaction. More precise observation of the C/E brings out the fact that there is a larger difference in C/E between A and B spectra for LIB90 than in those for REAC*63 and REAC*175. The large difference at the 14-MeV region between LIB90 and REAC*63&175 is attributed to the one order of magnitude lower cross sections in LIB90 than those in REAC*63 and REAC*175. Another discrepancy is found at the 0.2-keV region where LIB90 has no resonance and both REAC libraries exhibited large resonances. From this study, it is difficult to point out the source of large C/E values because the production is highly integrated over a wide energy range. Additional experiments using a different energy spectrum are recommended.

IV.D.4. ^{47}Sc

The radioactivity of ^{47}Sc is produced via the $^{51}V(n,n'\alpha)^{47}Sc$ and $^{50}V(n,\alpha)^{47}Sc$ reactions in vanadium. The latter reaction, however, plays a minor role due to the small abundance of ^{50}V (0.25%). In general, the reaction of $(n,n'\alpha)$ has a small cross section even at the 14-MeV energy region. JENDL and LIB90 give ~0.3 to 0.4 mb, whereas REAC*63 and REAC*175 have 11 and 7 mb, respectively. As there is no gamma ray associated with the ^{47}Sc decay, the difference among the libraries is shown in Fig. 11 by taking ratios to JENDL. As understood from the cross-section curve shown in Fig. 12, REAC*63 and REAC*175 give extremely large values. The validity of the cross section should be concerned. From the reaction systematics, in general, the $(n,n'\alpha)$ reaction tends to have at least one order of magnitude less cross section at 14 MeV than the (n,α) reaction cross section. As the cross section of $^{51}V(n,\alpha)$ being ~12 mb is validated by the ^{48}Sc production just before, the cross sections of 6.8 mb and 11.4 mb in REAC*175 and REAC*63, respectively, seem unreasonably large. Again, an experiment with explicit detection of ^{47}Sc is needed to judge the validity of the $(n,n'\alpha)$ reaction production.

IV.E. Chromium

IV.E.1. ^{49}Cr

The C/Es for A, the only case available, are shown in Fig. 13. The differences among the calculations are

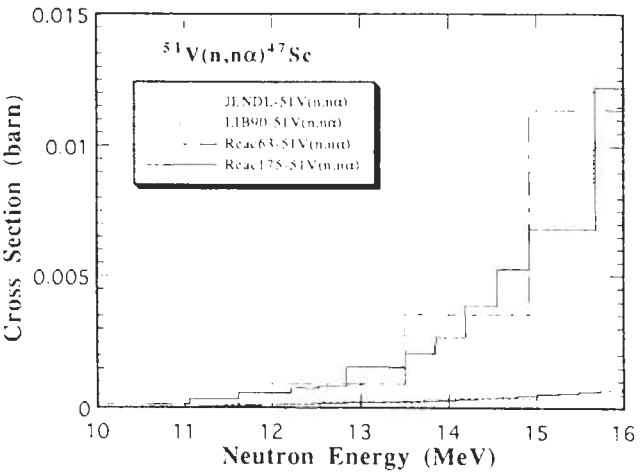

Fig. 12. Cross sections for the $^{51}V(n,\alpha)^{47}Sc$ in the four different libraries.

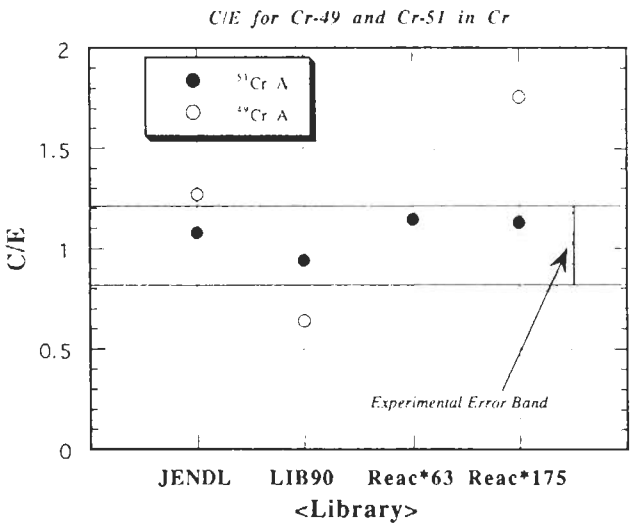

Fig. 13. The C/E values of isotopic radioactivities in chromium.

caused by the differences in cross sections at 14 MeV of each library. The overestimation by 50% in JENDL could not be explained by the inadequacy of the cross section because the cross sections ~14 MeV are in good agreement with the recent measurement at FNS (Ref. 44). We concluded that the correction for the sum peak counting loss for the gamma ray at 153 keV was not enough where the gamma-ray follows annihilation 511-keV gamma rays due to β^+ emission in the decay of ^{49}Cr. An examination for the correction factor is suggested to be verified directly using the sample of ^{49}Cr activity. Large overestimation with the C/E of 3 in REAC*63, even if the experimental value is revised, apparently is due to the extremely large cross section at 14.9 MeV. The REAC*175 value seems still slightly

overestimated. The cross section at the higher energy range from 14.5 MeV should be reevaluated.

IV.E.2. ^{51}Cr

The C/Es shown in Fig. 13 demonstrate the validity of the calculations in all libraries for all cases. The cross sections at 14 MeV in all libraries exhibited reasonable convergency. The activity of ^{51}Cr is produced mainly via $^{52}Cr(n,2n)^{51}Cr$, although the $^{50}Cr(n,\gamma)^{51}Cr$ reaction contributes to ^{51}Cr production by at most 1%. These consistent results for ^{51}Cr production indicate the validity of the $^{52}Cr(n,2n)^{51}Cr$ reaction cross section at 14 MeV as shown in Fig. 14.

IV.E.3. ^{49}V and ^{48}V

Since there was no observation for the radioactivities for ^{49}V and ^{48}V, only ratios of activities to JENDL were considered. All calculations are in good agreement for ^{49}V production. The cross section for the $^{50}Cr(n,np)$ reaction seems a reasonable range from the reaction cross-section systematics standpoint. For ^{48}V production, REAC*63 and REAC*175, however, are larger by factors of 5000 and 600 than JENDL. This is explained by the fact that the cross sections of $^{50}Cr(n,t)^{48}V$, which are considered the dominant reaction for the production of ^{48}V in REAC*63 and REAC*175 libraries are 35 and 0.2 mb, while only 1 mb in JENDL. In general, the (n,t) reaction cross section at the 14-MeV region is relatively small, being several millibarns at most. The cross sections in REAC libraries should be revised.

IV.E. Manganese and Copper

Elements of manganese and copper were studied simultaneously by using samples of manganese-copper alloy [Mn (80%), Cu (20%)]. As there are no similar radionuclides produced from each element, manganese and copper, we treated the isotopic radioactivity as those produced from only each element. The C/Es for manganese and copper are shown in Figs. 15 and 16, respectively.

IV.F.1. Manganese

IV.F.1.a ^{52}V. The ^{52}V is produced via the $^{55}Mn(n,\alpha)^{52}V$ reaction. JENDL and LIB90 agree with measurement within the experimental error. REAC*63 and REAC*175, however, slightly overestimated it by 25 and 16%, respectively. These differences are attributable to differences in the 14-MeV cross sections for the $^{55}Mn(n,\alpha)^{52}V$ reaction.

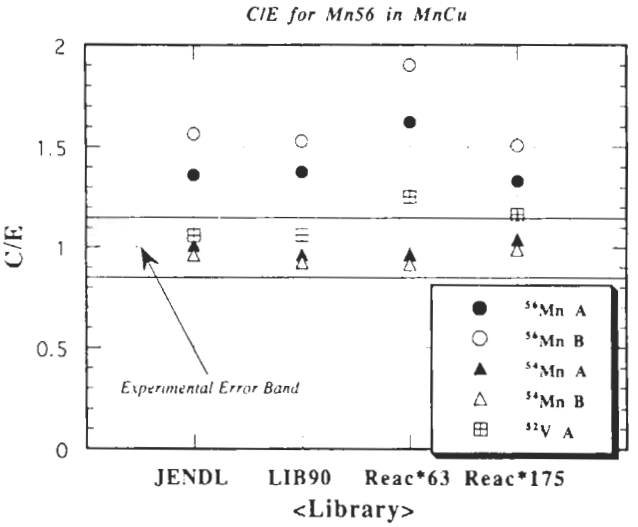

Fig. 15. The C/E values of isotopic radioactivities in manganese.

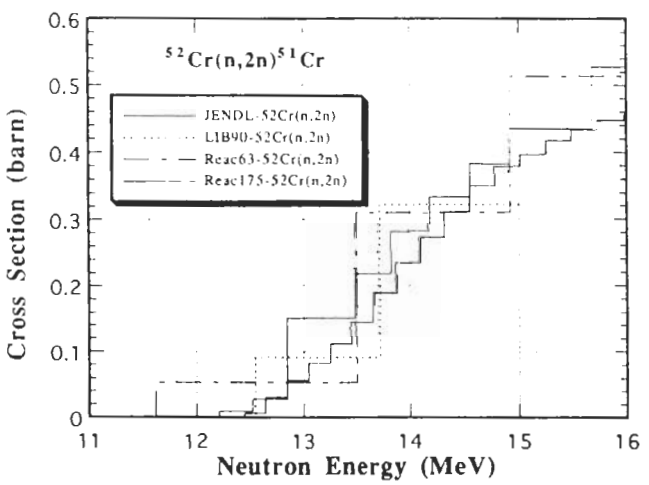

Fig. 14. Cross sections for the $^{52}Cr(n,2n)^{51}Cr$ in the four different libraries.

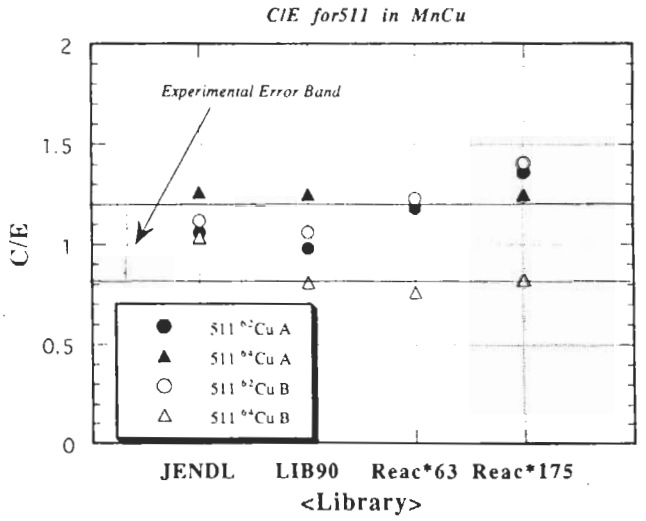

Fig. 16. The C/E values of isotopic radioactivities in copper.

IV.F.1.b. ^{54}Mn. All calculations with the four libraries predicted measurements well within experimental errors. Slight differences among the libraries are due to the cross sections at 14 MeV for the $^{55}Mn(n,2n)^{54}Mn$ reaction. The reaction cross-section values seem adequate.

IV.F.1.c. ^{56}Mn. The ^{56}Mn is produced via the $^{55}Mn(n,\gamma)^{56}Mn$ reaction in manganese. From the C/E shown in Fig. 15, all calculations overestimate the measurements by 20% to a factor of 2. The largest C/E value found in REAC*63 corresponds to the large resonance integral ~0.3 keV for the (n,γ) reaction. This factor will be discussed later. These systematical overestimations in all calculations may be caused by insufficient correction for the self-shielding of neutrons in the Mn-Cu alloy. The self-shielding of neutrons sensitive to ^{56}Mn production is enhanced by the $^{63}Cu(n,\gamma)$ reaction, which has a gigantic resonance at energy ~0.5 keV, just above the resonance of $^{55}Mn(n,\gamma)^{56}Mn$. Another possible source for the low experimental value is the insufficient sum peak correction factor for the experimental data. From those considerations, agreements should be improved over those presented in Fig. 15.

IV.F.2. Copper

IV.F.2.a. ^{62}Cu *and* ^{64}Cu. Both radioactivities of ^{62}Cu and ^{64}Cu are regarded as β^+ emitters, and 511-keV annihilation gamma rays dominate the gamma-ray spectrum. For the runs at short cooling times within 1 h, ^{62}Cu dominates the 511-keV gamma-ray intensity. For the cases with long irradiation and long cooling time, ^{62}Cu decays out and ^{64}Cu becomes major radionuclide. The C/Es are plotted in Fig. 16. Calculations overestimate the measurements by 40 to 80% for the short cooling cases in both A and B, which are very similar to that of ^{56}Mn, where samples were measured at close geometry to the detector. Meanwhile, recent measurements of $^{63}Cu(n,2n)^{62}Cu$ show that the cross-section value should be lower by 20% than the current evaluation. A new evaluation taking into account the recent measurements may mitigate this overestimation.

The systematic overestimation for the case of A by 20 to 25% seems to be affected by the insufficient correction of counting loss in the close detector-to-sample geometry. For the case of B, the sample of which was measured at the standard detector configuration, JENDL gives good agreement with the measurement, while the other libraries underestimate by 20 to 25%. These underestimations are partly due to lower cross-section values than found in JENDL. Another source arises in the lower contribution of $^{63}Cu(n,\gamma)^{64}Cu$ in the LIB90, REAC*63, and REAC*175 than that in JENDL, which amounts to 0.2 and 9% of the total production rate of ^{64}Cu for the spectra A and B, respectively.

IV.F.2.b. ^{62m}Co and ^{65}Ni. For ^{62m}Co production, JENDL has a problem showing extremely low C/E values below 0.2. The LIB90 and REAC*63 overestimate the measurements by 70 and 35%, respectively. All cross sections for $^{63}Cu(n,np)^{62m}Co$ should be reexamined. For ^{65}Ni production via the $^{65}Cu(n,p)^{65}Ni$ reaction, all calculations overestimate the measurement. It is difficult to point out the source of the discrepancies from the single measurement in spectrum A with the predominant 14-MeV neutron peak. Additional experimental measurement is desirable to test the validity for ^{65}Ni production.

IV.G. Iron

IV.G.1. ^{51}Cr *and* ^{54}Mn

As shown in Fig. 17, JENDL gives reasonable results for production of ^{51}Cr and ^{54}Mn. The underestimation for ^{51}Cr by REAC*63 is caused by the low cross sections of $^{54}Mn(n,\alpha)^{51}Cr$ at the 14-MeV region. The overestimation for ^{54}Mn by LIB90 is the result of the cross-section value at 14 MeV. The coarse energy group structure tends to give a larger value for the cross section with a descending profile in the 14-MeV region. It should be noted that the dependency of the neutron spectrum on the reaction rate around the 14-MeV region is sensitive to the mean energy of D-T neutron peak. More specific discussion will be given later.

IV.G.2. ^{56}Mn

The JENDL exhibited the best results for ^{56}Mn production. The C/E trend in each library as shown in Fig. 17 follows the differences in the reaction cross sections in each library, mainly for the $^{56}Fe(n,p)^{56}Mn$ reaction. The contribution of $^{57}Fe(n,np)^{56}Mn$ reaction is small due to a factor of 5 smaller cross section than

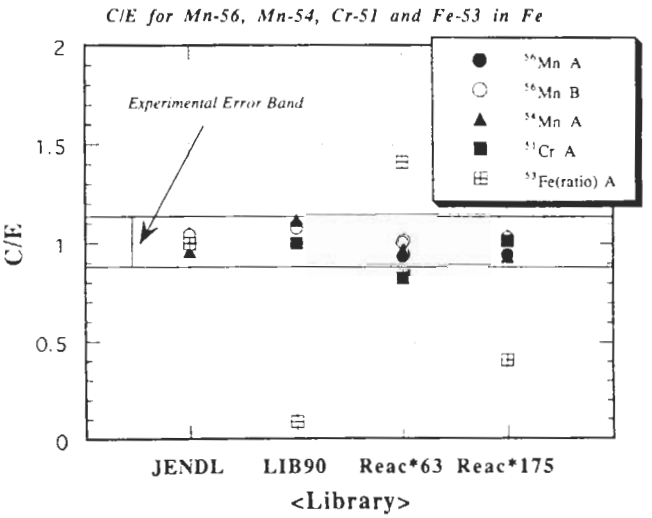

Fig. 17. The C/E values of isotopic radioactivities in iron.

the cross section of $^{56}Fe(n,p)$ and small abundance of ^{57}Fe in iron.

IV.G.3. ^{53}Fe

For the short-lived radionuclide ^{53}Fe ($T_{1/2}$ = 8.5 min), with production via the $^{54}Mn(n,2n)^{53m+g}Fe$ reaction, large discrepancies are found in the calculations of different libraries. The ratios to JENDL shown in Fig. 17 almost correspond to the ratio of the cross section at 14-MeV in each library. If the 511 annihilation gamma rays appeared in the gamma-ray spectrum for the case of A, it is due to the decay of ^{53}Fe. JENDL underestimated the ^{53}Fe by 30%. From this consideration, the cross section of REAC*63 seems most adequate.

IV.H. Cobalt

IV.H.1. ^{56}Mn

Figure 18 shows C/Es for ^{56}Mn, produced via the $^{59}Co(n,\alpha)^{56}Mn$ reaction. The C/E trends are reflected by the cross-section values at 14 MeV in each library. The range of the difference, however, is within 10% and the agreement of calculations with measurement are satisfactory. The best agreement is observed for JENDL. This is supported by the fact that the cross section of $^{59}Co(n,\alpha)^{56}Mn$ is in good agreement with recent experimental value at FNS (Ref. 44).

IV.H.2. ^{58}Co

The C/Es for ^{58}Co production are also given in Fig. 18. The cross-section curves are plotted in Fig. 19 for the reaction of $^{59}Co(n,2n)^{58m}Co$ and $^{59}Co(n,2n)$-^{58g}Co, which are the major contributors for ^{58}Co production. An overestimation observed in JENDL for the

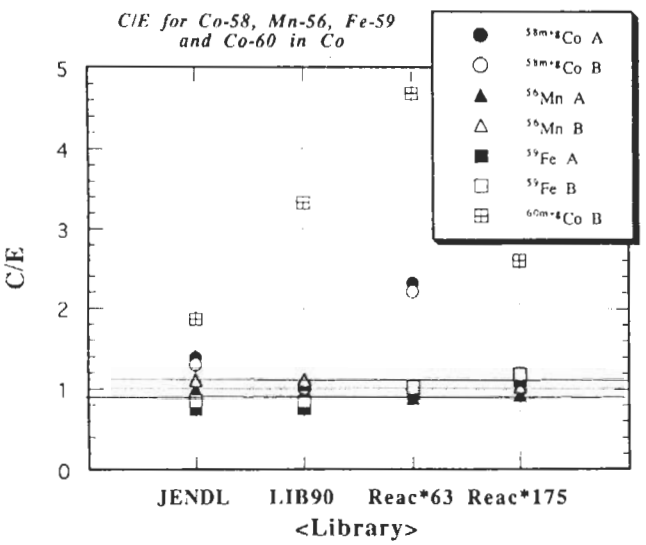

Fig. 18. The C/E values of isotopic radioactivities in cobalt.

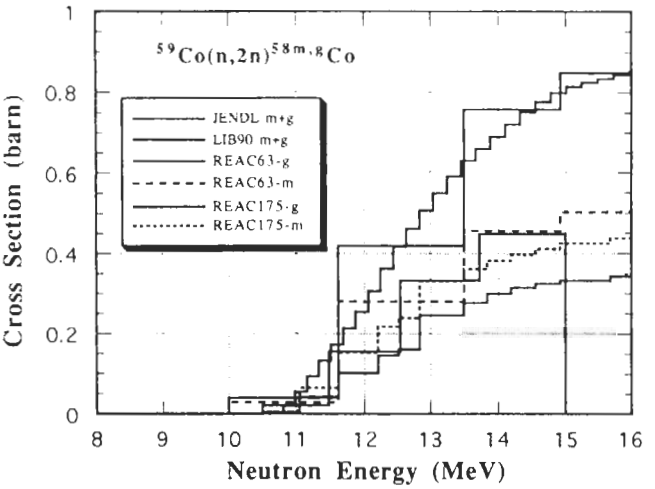

Fig. 19. Cross sections for the $^{59}Co(n,2n)^{58m,g}Co$ in the four different libraries.

case of A is attributable to the inadequacy of the ^{58}Co production cross section, which is given as $^{59}Co(n,2n)$-$^{58m+g}Co$. However, these reaction cross sections should be separately given because of the difference of the half-lives of these states. Since the isomer of ^{58}Co has the half-life of 9 h decaying to the ground state with 100% isomeric transition, the decay rate of ^{58}Co is time dependent due to the decay and growth relationship. Thus, the actual ^{58}Co decay rate must be less in general at a short cooling time. Thus, the overestimation in the JENDL is apparently explained. This situation could be mitigated for the case with long irradiation and long cooling. The large overestimations in REAC*63 are the result of the unreasonably large cross sections for both $^{59}Co(n,2n)^{58m}Co$, and $^{59}Co(n,2n)^{58g}Co$ reactions at 14 MeV. This situation is improved in REAC*175, giving reasonable agreement with measurement.

IV.H.3. ^{59}Fe and ^{60}Co

For ^{59}Fe, produced by the $^{59}Co(n,p)^{59}Fe$ reaction, all C/Es lie within a range from 0.85 to 1.08. There is not much difference between the results of spectra A and B. On the other hand, the production of ^{60}Co exhibits a scattered behavior among the libraries. The large discrepancies could be explained by the difference in the cross sections at the resonance region ~100 eV as well as ~14 MeV. Although JENDL gives the closest value to the measurement, still there is a strong overestimation by 80%. One possible reason for the overestimation is that there is less production of ^{60}Co due to strong self-shielding of neutrons via the $^{59}Co(n,\gamma)^{60}Co$ reaction, which has a gigantic resonance aroun 100 eV. From the energy sensitivity profile for spectrum B, >90% of the total ^{60}Co is born by the neutrons at this energy. A large self-shielding effect is reasonably expected.

IV.I. Nickel

IV.I.1. ^{57}Ni

As shown on Fig. 20, JENDL gives C/Es close to 1.0, while the other libraries tend to exhibit lower C/Es than 1.0. The cross sections of the $^{58}Ni(n,2n)^{57}Ni$ reaction strongly depend on the neutron energy in the 14-MeV region because of the high threshold energy at 12.5 and the steep excitation function of this reaction. When the D-T neutrons dominate the spectrum, the average evaluated cross section tends to be small. As long as D-T fusion neutron fields are present, the cross sections for the high threshold reaction such as $^{58}Ni(n,2n)^{57}Ni$ should be prepared with a sufficiently fine energy group structure. Otherwise, unreasonable underestimation or overestimation could easily occur. The validity of the JENDL calculation is also ensured by the fact that the cross section of this reaction in JENDL is consistent with the recent measurement at FNS (Ref. 44).

IV.I.2. ^{57}Co

The ^{57}Co is yielded from the direct reaction of $^{58}Ni[(n,np) + (n,d)]^{57}Co$ and the decay of the parent nuclide of ^{57}Ni, which is produced via the $^{58}Ni(n,p)$-^{57}Ni reaction. From the decay half-life of 36 h for ^{57}Ni, almost all ^{57}Co activities are produced via the direct reaction of $^{58}Ni[(n,np) + (n,d)]^{57}Co$ as far as this time range is concerned. Except REAC*63, calculations agree with the experiments within overall experimental uncertainty. JENDL treated the cross section as the sum of both (n,np) and (n,d), while other libraries separately give the cross sections for the two different channels. The overestimations in REAC*63 are caused by the one order of magnitude higher cross section for (n,d) reaction.

IV.I.3. ^{58}Co

As shown in Fig. 20, JENDL and REAC*175 are in good agreement with measurement. LIB90 and REAC*63, however, largely overestimate the experiments. It is found from Fig. 21 that there are unreasonably large overestimations in this cross section in libraries of LIB90 and REAC*63. This obviously gives unreasonably large C/Es. The difference in C/Es for cases with a long irradiation and cooling time between JENDL and REAC*175, however, should be noted. This is due to the difference in the isomer production cross section. At the short irradiation and cooling time, ^{58m}Co does not contribute to the ^{58}Co because of delay by the decay half-life of 9 h as discussed in ^{58}Co production in cobalt. However, $^{58}Ni(n,p)^{58m+g}Co$ should be considered in the case with a long irradiation and long cooling time. The overestimation in REAC*175 for case B indicates that the cross section of ^{58m}Co production is too large in the energy region <14 MeV.

IV.I.4. ^{60}Co

The ^{60}Co is one of the most important long-lived radionuclides. JENDL and REAC*175 underestimate measurement by 25 and 20%, respectively. This is reflected by the evaluation of the JENDL-3 cross section, which is lower by 20% than the recent experimental value at FNS (Ref. 44). The cross section of REAC*175 seems lower than the current experimental value by 20%. When the cross sections are revised by using the new experimental value, better agreement could be achieved. The overestimation of LIB90 by 20% is explained by the large cross section value at 14 MeV being 180 mb, which is 20% larger than the experimental value of 150 mb. The best agreement is observed in REAC*63, even though the cross section in the library seems too coarse.

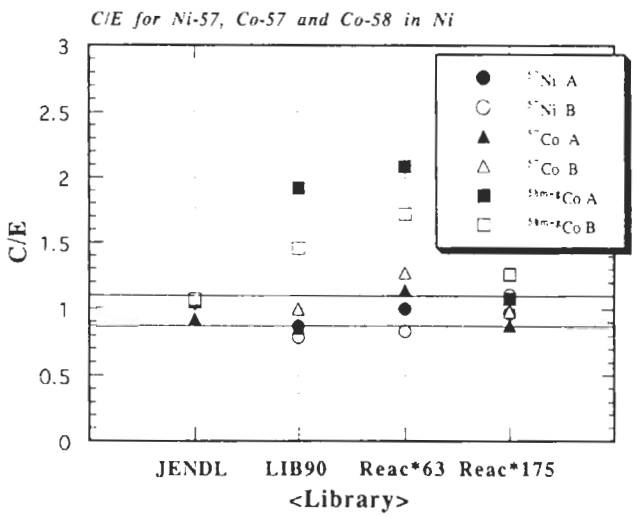

Fig. 20. The C/E values of isotopic radioactivities in nickel.

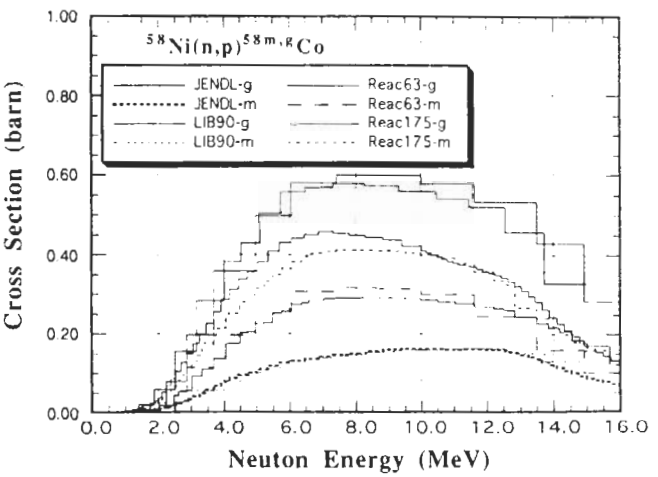

Fig. 21. Cross sections for the $^{58}Ni(n,p)^{58m,g}Co$ in the four different libraries.

IV.I.5. ^{65}Ni and ^{62m}Co

Concerning ^{65}Ni production, only ratios to JENDL are shown in Table III. REAC*63 shows a factor of two larger value than those of other libraries.

For ^{62m}Co production, JENDL has a problem giving a C/E of 5 as given in Table III. This cannot be explained by the difference in the cross sections at 14 MeV. Other possible sources in the decay chain and gamma-ray yield libraries should be investigated. An overestimation by a factor of 2.7 in REAC*63 is attributable not only to the large cross section of ^{62}Ni$(n,p)^{62m}$Co at 14 MeV, but to the unreasonably high cross section of the ^{64}Ni$(n,t)^{62m}$Co reaction in the library. The ratio of C/E in REAC*175 to that in LIB90 corresponds to the ratio of the cross section of ^{62}Ni$(n,p)^{62m}$Co at 14 MeV in the REAC*175 library to that in LIB90.

IV.J. Type 316 Stainless Steel

It should be noted that there were some discrepancies between the atomic densities of the elements composing the Type 316 stainless steel used in the ACT4 calculations (JENDL and LIB90) and the REAC calculations (REAC*63 and REAC*175). In Table IV, the atomic densities of major elements are listed to show the differences that have to be taken into account in the following C/E discussion. The C/E values are shown in Figs. 22a and 22b.

IV.J.1. ^{56}Mn

The C/E trend is similar to that in iron. Large differences in abundance of manganese, as indicated in Table IV, is considered not to be a large factor. For the case of the softer spectrum, the contribution of ^{55}Mn$(n,\gamma)^{56}$Mn to ^{56}Mn production is at most 10% of the contribution of ^{56}Fe$(n,p)^{56}$Mn if the neutron flux spectrum B and cross sections of JENDL for these reactions are assumed. The importance of manganese, however, increases in a different neutron spectrum at a deeper location with <14-MeV neutron fraction or in a thermalized spectrum. In this viewpoint, another new measurement in the well-defined spectrum is highly desirable to demonstrate the validity of the calculations.

IV.J.2. ^{54}Mn

On the contrary to ^{56}Mn production, the manganese constituent plays an important role for ^{54}Mn production through the ^{54}Mn$(n,2n)^{54}$Mn reaction, the effective cross section is comparable to that of the ^{54}Fe$(n,p)^{54}$Mn reaction in iron. The drastic underestimations in REAC*63 and REAC*175 are understandable given the lower fraction of manganese by a factor of 6 than that used in the calculations of JENDL and LIB90. All C/Es, however, underestimate the measured activity beyond the uncertainty of ±10% in the abundance, which is expected from the variation of the fraction of the element.

IV.J.3. ^{51}Cr and ^{49}Cr

Though all of C/Es for ^{51}Cr in chromium are close to 1.0, the C/Es in stainless steel are systematically lower than 1.0, as illustrated in Fig. 22b. Since there is no other possible reaction channel to produce ^{51}Cr in the composition, the abundance of chromium could be underestimated in the calculation. The trend of C/Es for ^{49}Cr production is very similar to that in the analysis of chromium. Thus, the underestimation of the chromium constituent in the stainless sample is also supported.

IV.J.4. ^{58}Co, ^{57}Co, and ^{57}Ni

The C/E trends for these radionuclides are consistent with those in nickel as shown in Figs. 22a and 22b. Therefore, the abundance of nickel seems adequate even though the data are different for the ACT4 and REAC calculations.

TABLE IV

Comparison of Atomic Densities of Major Elements in Type 316 Stainless Steel Used in ACT4 and REAC*3 Calculations

Element	Atomic Density (atom/cm^3)		Ratio ACT4/REAC*3
	ACT4 (JENDL and LIB90)	REAC*3 (REAC*63 and REAC*175)	
Iron	5.8947E+22[a]	5.5687E+22	1.0585
Chromium	1.3651E+22	1.4690E+22	0.9293
Nickel	1.0968E+22	1.1113E+22	0.9870
Molybdenum	1.2805E+21	1.2173E+21	1.0519
Manganese	1.0000E+21	1.5804E+20	6.3275

[a]Read as 5.8947×10^{22}.

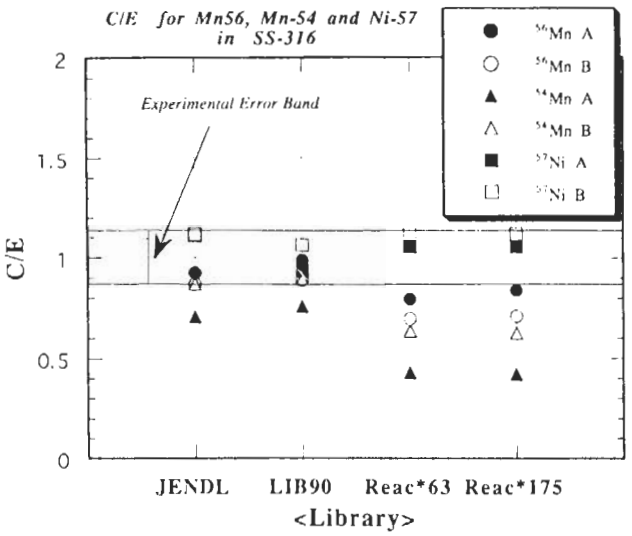

Fig. 22a. The C/E values of isotopic radioactivities in Type 316 stainless steel.

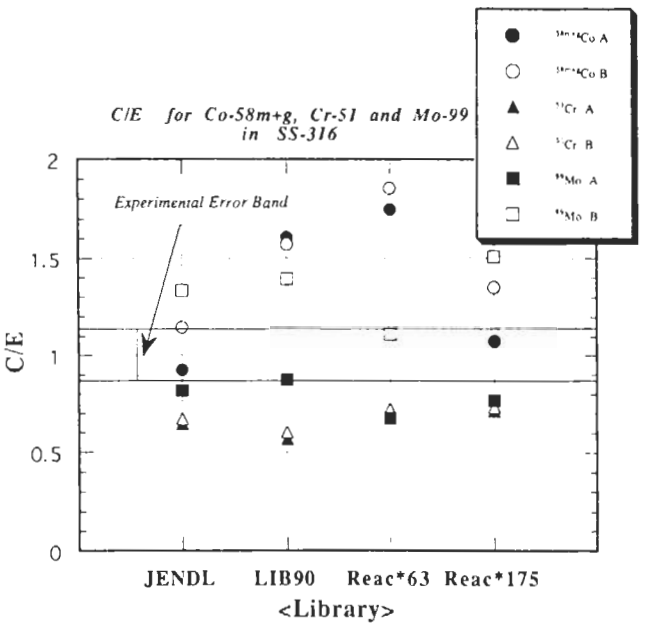

Fig. 22b. The C/E values of isotopic radioactivities in Type 316 stainless steel.

IV.K. Niobium

IV.K.1. ^{92m}Nb

Although niobium is not a primary structural material, the reaction of $^{93}Nb(n,2n)^{92m}Nb$ is considered as an important dosimeter in the D-T neutron flux dosimetry. The results for experimental analysis of niobium are thoroughly given in the companion paper.[40] A highlight is given here in order to give another assurance for the neutron spectrum used in the analysis.

The C/Es are shown in Fig. 23. The best agreement is found in LIB90. JENDL slightly overestimates the measurement by 4 to 8%. REAC*63 and REAC*175 show higher overestimation than JENDL by 8 to 10%. The cross section of the $^{93}Nb(n,2n)^{92m}Nb$ reaction at the 14-MeV region has been extensively studied, and a value 459 mb is recognized to be a convergent cross section for the reaction.[43] Figure 24 is a comparison of the cross section in the different libraries. According to this value, the C/E trend can be explained directly. The cross section of more than 500 mb in REAC*175 seems out of the range for this reaction. When the reaction cross sections are to be replaced with the currently assessed cross-section value, better agreement can

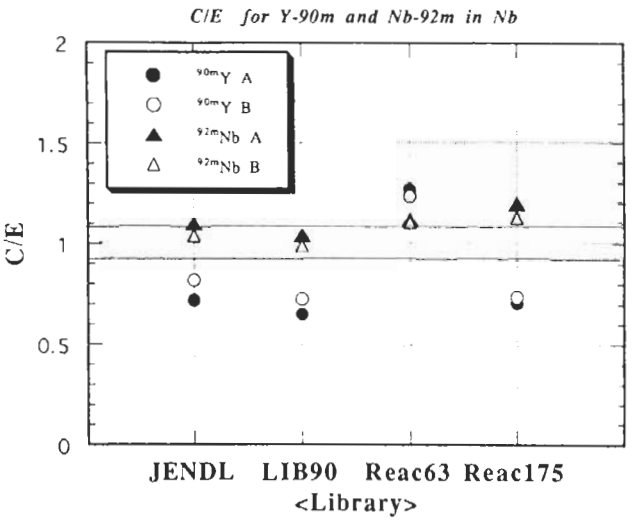

Fig. 23. The C/E values of isotopic radioactivities in niobium.

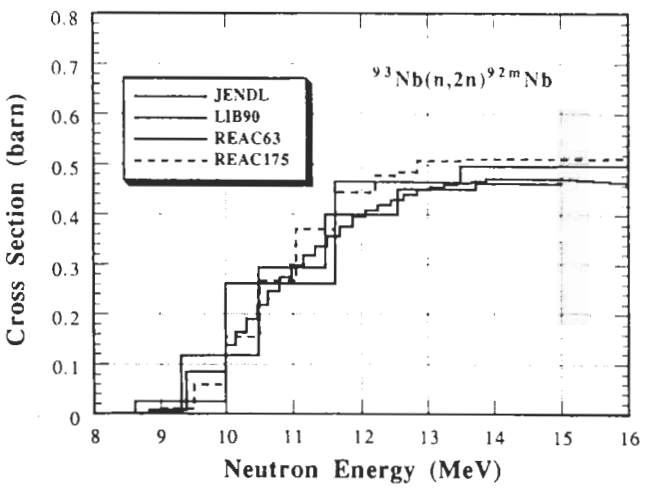

Fig. 24. Cross sections for the $^{93}Nb(n,2n)^{92m}Nb$ in the four different libraries.

be achieved. In this context, the validity of the neutron fluxes employed in the calculations are ensured.

IV.K.2. ^{90m}Y

The ^{90m}Y, a product of the $^{93}Nb(n,\alpha)^{90m}Y$ reaction, is another major radionuclide in niobium at a short cooling time. Three libraries, JENDL, LIB90, and REAC*175 show underestimation by ~30%, whereas REAC*63 overestimates experiments by >20%. According to the recent experimental data,[41] the cross section at ~14 MeV falls in the range of 4.9 to 5.4 mb. The corresponding cross sections in JENDL, LIB90, and REAC*175 are in a range from 3 to 3.5 mb. On the other hand, the cross section in REAC*63 is ~9 mb at 14.5 MeV. Thus, it is understood that these overestimations and underestimations are directly related to the cross-section values at 14 MeV. Reevaluation is suggested for the cross sections in all libraries investigated.

V. DISCUSSION

V.A. Overall C/E Trend

V.A.1. General Trend

All the C/Es are plotted in Fig. 25 to give the uncertainty ranges of the radioactivity calculations. Almost all C/Es fall in between 0.5 and 1.5, though some of them are peculiarly large, exceeding a factor of 5 and <0.1. From the previous discussion on each radionuclide, it was concluded that some cross sections are physically unreasonably installed in the library. Especially, several orders of magnitude difference was found in the cross sections for rare exotic reactions, e.g., $(n,2p)$ and $(n,n'\alpha)$. On the other hand, a small C/E indicates that there are no corresponding cross sections in spite of the importance of the reactions. As this experimental analysis demonstrates the importance of both sides, completeness and quality, both aspects should be taken into account. To explain the disagreement, sometimes it is necessary to look into all the possible reaction channels, even though these reactions are most unlikely to take place. To meet the requirements for completeness, we have to rely on a model calculation based on some theoretical approach or reaction systematics available. In general, these prediction methods are reliable when sufficient experimental data are available. However, it was proved that it is very dangerous to fully rely on the calculations.

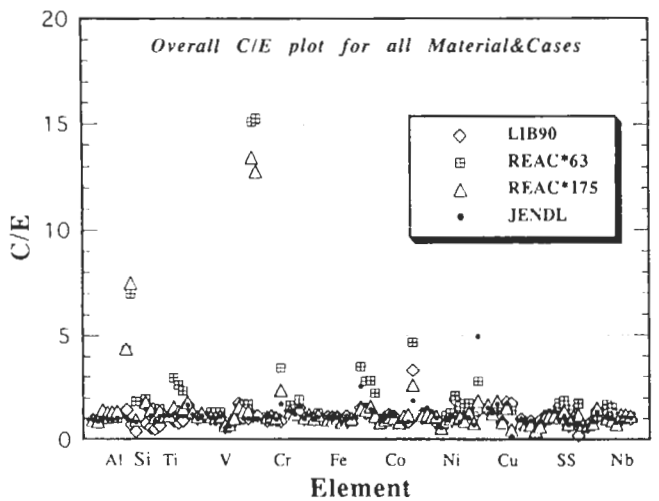

Fig. 25. The overall C/E plot.

V.A.2. C/E Distribution

The validity of the currently available cross-section libraries has been examined through the C/E in the fusion neutron environment. The total number of cases is 95 on 44 reaction products for 12 elements that were considered according to the data in Table III. Figures 26 through 29 show more specific C/E distributions given as $(C - E)/E$ for JENDL, LIB90, REAC*63, and REAC*175, respectively. The C/E distribution for JENDL exhibits a very sharp peak in the number of cases. Except for one case showing a deviation of a factor of 4, all calculations show deviations from measurements a factor of <2. There is also a peak around the center $[(C - E)/E = 0]$ in LIB90's distribution. It, however, gives a distribution broadened profile. Contrary to rather symmetric distributions in JENDL and LIB90, deviations in REAC*63 show a distorted distribution. A tail in the positive region indicates that REAC*63 tends to give overestimations. The distribution of REAC*175 seems similar to that of LIB90. As long as this study is concerned, it is concluded that JENDL with the 125 energy group structure is the best in quality among the library tests. Although REAC*175 is assumed to be based on an updated cross-section database, it is pointed out that there is still a need to improve its quality. LIB90 showed a modest result; however, the data are insufficient and should be replaced with the more realistic data of JENDL. REAC*63 now should be substituted with the new version of REAC*175 for fusion applications.

V.B. Uncertainty Consideration

V.B.1. Uncertainty in Experimental Data

Experimental error assessment is the starting point to evaluate C/Es. Here, the experimental error is outlined to give a fundamental idea of the uncertainty range in the C/E consideration. For the quantity of radioactivity intensity per gram, per normalized source intensity, as given in Eq. (2), the major sources of experimental error include (a) statistical error for the

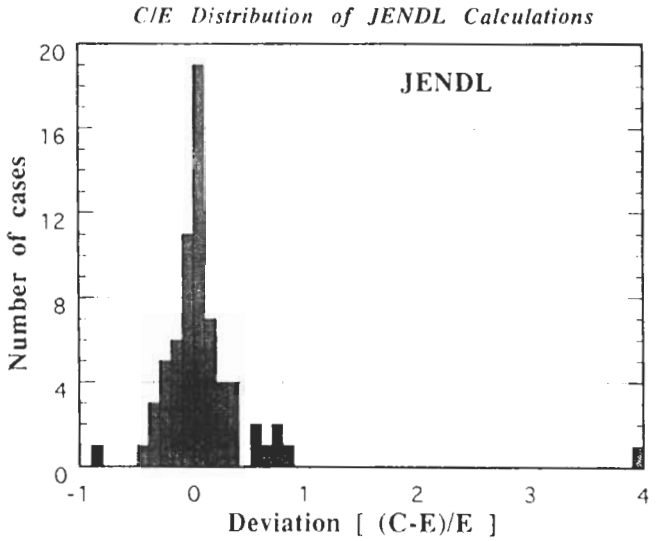

Fig. 26. The C/E distribution for JENDL.

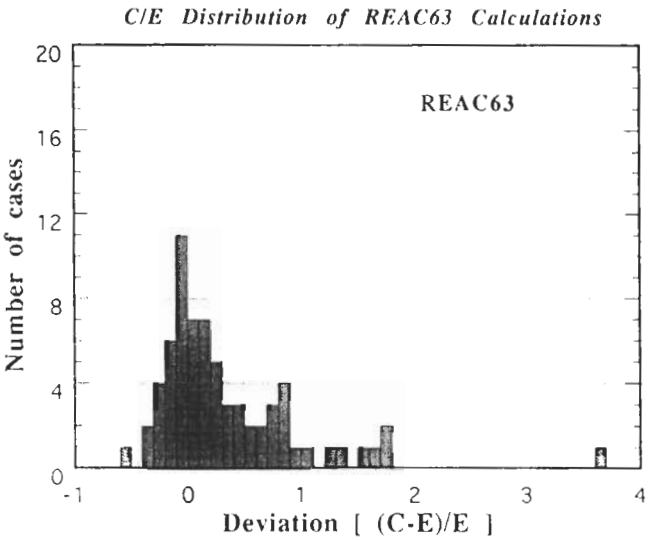

Fig. 28. The C/E distribution for REAC*63.

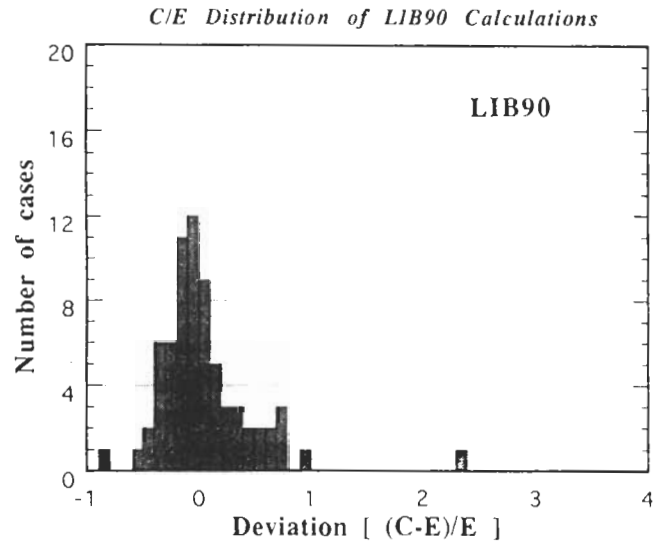

Fig. 27. The C/E distribution for LIB90.

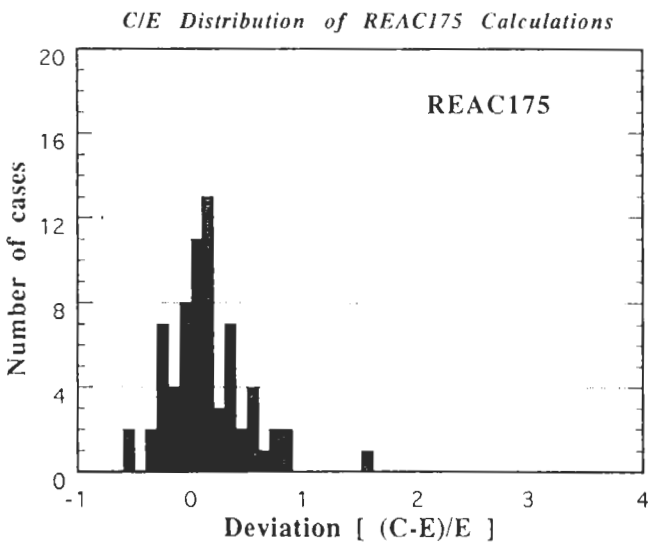

Fig. 29. The C/E distribution for REAC*175.

gamma-ray peak counts of interest, (b) error of gamma-ray detector efficiency, and (c) neutron yield at the source. In this study, some of the gamma-ray results with poor statistics were shown in order to provide data with reasonable accuracy, even though the activities of these gamma rays were identified. In general, errors due to counting statistics were less than ±10%, in many cases, less than ±5%. The error associated with the gamma-ray detector efficiency normally was assigned to ±3%. In the measurement, multiple relative gamma-ray detectors were employed to make consecutive counts of plural samples. Thus, additional errors due to efficiency calibrations should be considered. The error of the neutron yield was less than ±2%. As a result, the overall experimental error ranged from ±5 to 15% in most cases.

V.B.2. Uncertainty in the Calculation

In general, the coarse energy group structure tends to offer results less sensitive to the neutron energy spectrum, averaging the cross section in a broad energy interval. For example, the reaction rate calculations for reactions with steep excitation functions ~14 MeV require careful treatment for cross-section averaging. Figure 30 illustrates changes of reaction rate with a change of the mean D-T peak energy for three representative $(n,2n)$ reactions: the $^{46}Ti(n,2n)^{45}Sc$, $^{58}Ni(n,2n)^{57}Ni$

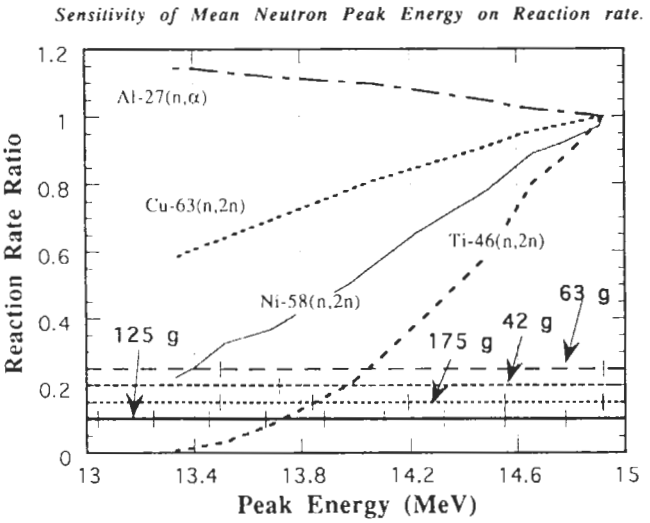

Fig. 30. Changes in reaction rates for high-energy threshold reactions with respect to neutron energy changes.

and $^{63}Cu(n,2n)^{62}Cu$, and the $^{27}Al(n,\alpha)^{24}Na$ reactions. The calculations are based on the JENDL library with 125-energy-group structure. The neutron energy spectra at different emission angles, calculated with the MORSE-DD for the rotating neutron target system, were used in this analysis. In Fig. 30, boundaries of the other energy group structures are shown. The finest energy structure in the energy region ~14 MeV is found in JENDL, even the total number of groups, 125, is less than the 175 groups in REAC*175. This figure demonstrates that calculation with coarse group structures can be insensitive to changes of the neutron spectrum. For a D-T fusion reactor, we can assume that the mean D-T neutron peak energy is close to 14.1 MeV. Most of the multigroup libraries have been prepared based on this assumption. In general, the peak energy of the accelerator-based D-T neutron source is strongly dependent on the angle of the sample position with respect to the incident d^+ beam energy, as in the case of the current experiment at FNS. In this case, we have to use the fine neutron spectrum as the weighting function to prepare the cross sections with coarse energy structure. This seems impractical. Thus, it is recommended to use an energy group structure as fine as possible in the activation calculation. Recent developments of computers with high speed, large disk space, and less expense mitigate the difficulty of running a code system with a fine energy group structure such as 125 and 175 groups.

Another uncertainty, we must consider, is associated with the transport calculation of the neutron flux. Throughout this examination, we assume that spectra A and B are well defined with certain accuracy. For the high-energy part, in fact, validity of these spectra was ensured from the excellent agreement between the calculations and experiments for radioactivities of the ^{24}Na and ^{92m}Nb, production cross sections of which are considered to be the most reliable. The reasonably good agreement of the MORSE-DD calculation with the measurement for the $^{115}In(n,n')^{115m}In$ reaction rate[45] also demonstrated the validity of the calculation in the mega-electron-volt region of the neutron flux. Thus, the uncertainty range of ±10% could be ensured for the neutron fluxes in the energy range >1 MeV from the considerations of the C/E values as well as the cross-section uncertainties for the dosimetry reactions.

However, it is extremely difficult to quantify the uncertainty range of the neutron flux below 0.1 MeV because there was no effective verification with the appropriate dosimetry reactions. Only the MORSE-DD calculation was tested by the reaction rate of the $^{197}Au(n,\gamma)^{198}Au$ reaction.[46] The results suggested that the calculation tended to underestimate the reaction rate measured on the surface of the cavity by 10 to 20%. This range of underestimation for the $^{197}Au(n,\gamma)$-^{198}Au reaction rate suggested that the neutron flux spectrum used in this analysis is also lower than the actual flux level in the low-energy region. Thus, we must take into account an uncertainty rage of ±20% in the analysis for the (n,γ) reaction products. Figures 31 and 32 give the differential sensitivities of reaction rates derived by multiplying reaction cross sections in JENDL and the spectra A and B, respectively, for representative (n,γ) reactions, $^{63}Cu(n,\gamma)^{64}Cu$, $^{55}Mn(n,\gamma)^{56}Mn$, and $^{59}Co(n,\gamma)^{60}Co$. It is found that in both spectra, the neutron flux in the resonance energy region contributes predominantly to the total reaction rate. In particular, >70% contribution is presented from that flux. In Table V, calculated reaction rates and fractional contributions from the resonance and 14-MeV energy regions are tabulated for those three reactions. As seen, large differences among the calculations of the four libraries were observed, not only in the total reaction

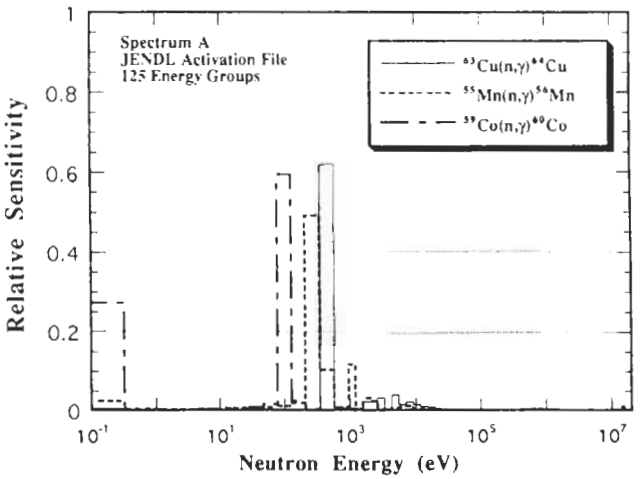

Fig. 31. Differential sensitivities of the (n,γ) reactions for spectrum A.

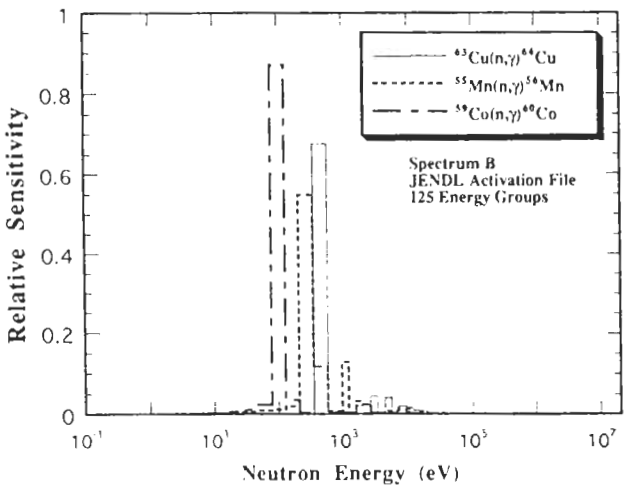

Fig. 32. Differential sensitivities of the (n,γ) reactions for spectrum B.

rate, but also in the fractional contributions. These discrepancies are partly attributable to the differences in the energy group structures and partly due to the differences in the cross-section values themselves. Therefore, in this test, there should be allowances for further discussion on the dominant radionuclides produced by the (n,γ) reactions.

VI. CONCLUSION

Precise analysis of induced radioactivities in the structural materials for D-T fusion reactor components were conducted in order to examine the adequacy of activation cross-section libraries, which are commonly used or are utilized in neuronic calculations for comprehensive reactor design analysis. The JENDL activation library and the REAC*3 library were thoroughly tested by using broad experimental data obtained under the framework of JAERI/U.S. DOE collaboration.

We found that almost all deviations of calculations from experiments can be attributed directly to inadequacy in the activation cross sections or improper treatment of decay chains. The requirement of "completeness" for an activation cross-section library has to be satisfied by theoretical calculation or systematic estimation for rare reactions for which there are no experimental data. The outcome of this work clearly provides direct information on the deficiency of the cross sections and inadequacy of these values. We are encountering a crucial decision on which library should be taken as the foremost data library and which is well validated for the critical design of ITER or DEMO. If the validation is the foremost issue in adopting the library, the JENDL activation library would be the best choice as far as the libraries tested in this study. The weakness of JENDL is characterized by its incompleteness for covering all physically possible reactions. However, the effort is still vigorously in progress. The final version of JENDL, no doubt, will satisfy both requirements. REAC*175 seems the most preferable library among the libraries tested here, at present, from the "completeness" requirement point of view with sufficient energy group structure. However, as pointed out in this study, there are a lot of unreasonable implementations of cross sections, even though they are well known and frequently appear in the radioactivity calculations. When the cross sections are revised based on the suggestions made in this work, the REAC*175 will be the best library from the completeness point of view.

TABLE V

Total Reaction Rates and Fractions of Resonances and 14 MeV for $^{63}Cu(n,\gamma)^{64}Cu$, $^{55}Mn(n,\gamma)^{56}Mn$, and $^{59}Co(n,\gamma)^{60}Co$

Library	$^{63}Cu(n,\gamma)^{64}Cu$			$^{55}Mn(n,\gamma)^{56}Mn$			$^{59}Co(n,\gamma)^{60}Co$			
	Total	Resonance	14 MeV	Total	Resonance	14 MeV	Total	Resonance	14 MeV	Thermal
Spectrum A										
JENDL	3.154E−05[a]	0.63	0.003	3.141E−05	0.822	0.034	1.307E−04	0.65	0.024	0.274
LIB90	2.178E−05	0.76	0.008	3.178E−05	0.745	0.034	1.168E−04	0.84	0.002	0.002
REAC63	2.507E−05	0.49	0.184	3.843E−05	0.785	0.036	2.001E−04	0.44	0.008	0.013
REAC175	2.693E−05	0.46	0.156	3.155E−05	0.767	0.033	1.292E−04	0.89	0.011	0.027
Spectrum B										
JENDL	2.213E−05	0.69	0.000	2.153E−05	0.908	0.000	6.621E−05	0.95	0.000	0.000
LIB90	1.462E−05	0.85	0.000	2.104E−05	0.837	0.000	7.779E−05	0.95	0.000	0.000
REAC63	1.357E−05	0.68	0.003	2.684E−05	0.816	0.000	1.442E−04	0.96	0.000	0.000
REAC175	1.512E−05	0.61	0.003	2.127E−05	0.863	0.000	9.144E−05	0.94	0.000	0.000

[a]Read as 3.154×10^{-5}.

ACKNOWLEDGMENTS

Authors wish to acknowledge J. Kusano, C. Kutukake, S. Tanaka, and Y. Abe for operation of the FNS accelerator.

The U.S. contributors were supported by the U.S. Department of Energy, Office of Fusion Energy, under contract DE-FG03-86ER52123.

REFERENCES

1. S. BLOW, "Some Features of the Behaviour of Structural Materials in a Possible Fusion Reactor Blanket," AERE-R 6845, U.K. Atomic Energy Research Establishment, Harwell (1971).

2. W. F. VOGELSANG, G. L. KULCINSKI, R. G. LOTT, and T. Y. SUNG, "Transmutations, Radioactivity, and Afterheat in a Deuterium-Tritium Tokamak Fusion Reactor," *Nucl. Technol.*, **22**, 379 (1974).

3. D. J. DUDZIAK and R. A. KRAKOWSKI, "Radioactivity Induced in a Theta-Pinch Fusion Reactor," *Nucl. Technol.*, **25**, 32 (1975).

4. R. W. CONN, T. Y. SUNG, and M. A. ABDOU, "Comparative Study of Radioactivity and Afterheat in Several Fusion Reactor Blanket Designs," *Nucl. Technol.*, **26**, 391 (1975).

5. M. L. WILLIAMS, R. T. SANTORO, and T. A. GABLIEL, "The Calculated Performance of Various Structural Materials in Fusion-Reactor Blankets," *Nucl. Technol.*, **29**, 384 (1976).

6. W. F. VOGELSANG, "Radioactivity and Associated Problems in Thermo-Nuclear Reactors," UWFDM-178, University of Wisconsin, Madison (1976).

7. E. E. BLOOM et al., "Low Activation Materials for Fusion Applications," *J. Nucl. Mater.*, **122 & 123**, 17 (1984).

8. R. W. CONN et al., "Lower Activation Materials and Magnetic Fusion Reactors," *Nucl. Technol./Fusion*, **5**, 291 (1984).

9. G. LOGAN, "A Rationale for Fusion Economics Based on Inherent Safety," *J. Fusion Energy*, **4**, 245 (1985).

10. T. NODA et al., "Materials Selection for Reduced Activation of Fusion Reactors," *J. Nucl. Mater.*, **155–157**, 581 (1988).

11. L. R. GREENWOOD and D. L. BOWERS, "Production of Long-Lived Activities in Fusion Materials," *J. Nucl. Mater.*, **155–157**, 585 (1988).

12. E. T. CHENG, "Radioactivity Aspects of Fusion Reactors," *Fusion Eng. Des.*, 8 (1989).

13. M. ZUCCHETTI, "Impurity Concentration Limits and Activation in Fusion Reactor Structural Materials," *Fusion Technol.*, **19**, 294 (1991).

14. E. T. CHENG, K. M. FENG, R. FORREST, J. H. HUANG, J. KOPECKY, F. M. MANN, A. V. KASHIRSKIJ, D. V. MARKOVSKIJ, O. SCHIPAKIN, M. SAWAN, and Y. SEKI, "International Fusion Activation Calculation Comparison Study," TSIR-12 (1991).

15. Y. IKEDA, Y. SEKI, H. MAEKAWA, Y. OYAMA, and T. NAKAMURA, "Measurements of Induced Activity in Type 316 Stainless Steel by Irradiation in D-T Neutron Fields," *Fusion Technol.*, **8**, 1466 (1985).

16. T. NAKAMURA, H. MAEKAWA, Y. IKEDA, Y. OYAMA, and J. KUSANO, "Present Status of the Fusion Neutronics Source (FNS)," *Proc. 4th Symp. Accelerator Sci. Technol.*, Riken, Japan, November 24–26, 1982. p. 155.

17. T. NAKAMURA and M. A. ABDOU, "Summary of Recent Results from the JAERI/U.S. Fusion Neutronics Phase-I Experiments," *Fusion Technol.*, **10**, 541 (1986).

18. H. MAEKAWA and M. A. ABDOU, "Overview of the Latest Experiments Under the JAERI/USDOE Collaborative Program on Fusion Neutronics," *Fusion Des. Eng.*, **18**, 275 (1991).

19. T. NAKAMURA et al., "A Line D-T Neutron Source Facility for Annular Blanket Experiment: Phase III of the JAERI/USDOE Collaborative Program on Fusion Neutronics," *Fusion Technol.*, **19**, 1873 (1991).

20. Y. OYAMA et al., "Annular Blanket Experiment Using a Line D-T Neutron Source: Phase IIIA of the JAERI/USDOE Collaborative Program on Fusion Neutronics," *Fusion Technol.*, **19**, 1879 (1991).

21. Y. OYAMA et al., "Phase III Experimental Results of JAERI/USDOE Collaborative Program on Fusion Neutronics," *Fusion Eng. Des.*, **18**, 203 (1991).

22. F. M. MANN, "REAC*2: Users Manual and Code Description," WHC-EP-0282, Westinghouse Hanford Company (1989).

23. Y. SEKI et al., "THIDA-2: An Advanced Code System for Calculation of Transmutation, Activation, Decay Heat and Dose Rate," RSIC computer code collection, CCC-410, Oak Ridge National Laboratory (Apr. 1987).

24. D. L. HENDERSON and O. YASAR, "A Radioactivity and Dose Rate Calculation Code Package," Vols. 1 and 2, RSIC computer code collection, CCC-323, Oak Ridge National Laboratory (Apr. 1987).

25. J. JUNG, "Theory and Use of the Radioactivity Code RACC," ANL/FPP/TM-122, Argonne National Laboratory (1979).

26. A. KUMAR, M. A. ABDOU, Y. IKEDA, and C. KONNO, "Radioactivity and Nuclear Heating Measurements for Fusion Applications," *Fusion Technology 1990*, p. 872, B. E. KEEN, M. HUGUET, and R. HEMSWORTH, Eds., Elsevier Science Publishers B.V., Amsterdam (1991).

27. Y. IKEDA, C. KONNO, T. NAKAMURA, A. KUMAR, and M. A. ABDOU, "Experiment on Induced Activities and Decay-Heat in Simulated D-T Neutron Fields: JAERI/USDOE Collaborative Program on Fusion Neutronics," *Fusion Technol.*, **19**, 1961 (1991).

28. A. KUMAR, M. A. ABDOU, Y. IKEDA, and T. NAKAMURA, "Analysis of Induced Activities Measurements Related to Decay-Heat in Phase IIC Experimental Assembly: USDOE/JAERI Collaborative Program on Fusion Neutronics Experiments," *Fusion Technol.*, **19**, 1909 (1991).

29. A. KUMAR, M. Z. YOUSSEF, Y. IKEDA, C. KONNO, and Y. OYAMA, "Experiments and Analysis for Measurements of Decay-Heat Related Induced Activities in Simulated Line Source Driven D-T Neutron Fields of Phase IIIA: USDOE/JAERI Collaborative Program on Fusion Neutronics," *Fusion Technol.*, **19**, 1859 (1991).

30. Y. IKEDA, C. KONNO, Y. OYAMA, T. NAKAMURA, A. KUMAR, M. Z. YOUSSEF, and M. A. ABDOU, "Experimental Verification of the Current Data and Methods for Induced Radioactivity and Decay Heat Calculation in D-T Fusion Reactors," *Fusion Eng. Des.*, **18**, 387 (1991).

31. Y. IKEDA, A. KUMAR, and C. KONNO, "Measurements of Long-lived Activation Cross Sections by 14 MeV Neutrons at FNS," presented at Int. Conf. Nuclear Data on Science and Technology, Jülich, Germany, May 1991; see also *Proc. Int. Workshop Fusion Neutronics*, Karlsruhe, Germany, June 7, 1991, JAERI-memo 03-305, p. 172, Japan Atomic Energy Research Institute (Sep. 1991).

32. A. KUMAR et al., "Measurements of Decay Radioactivity of Long-Lived Isotopes," *Fusion Technol.*, **21**, 2180 (1992).

33. Y. NAKAJIMA, "JENDL Activation Cross Section File," JAERI-M 91-032, p. 43, Japan Atomic Energy Research Institute (1991).

34. F. M. MANN, "REAC*3 Nuclear Data Libraries," *Proc. Int. Conf. Nucl. Data Sci. Technol.*, Jülich, Germany, May 12–17, 1991, p. 936.

35. Y. OYAMA et al., "Phase-IIC Experiments of the USDOE/JAERI Collaborative Program on Fusion Blanket Neutronics—Experiments and Analysis of Heterogeneous Fusion Blanket—Vol-I: Experimental Results," JAERI-M 92-183, UCLA-FTN-64, UCLA-ENG-93-19, Japan Atomic Energy Research Institute (1992).

36. M. NAKAGAWA et al., "Phase-IIC Experiments of the USDOE/JAERI Collaborative Program on Fusion Blanket Neutronics—Experiments and Analysis of Heterogeneous Fusion Blanket—Vol-II: Analysis," JAERI-M 92-183, UCLA-FTN-64, UCLA-ENG-93-19, Japan Atomic Energy Research Institute (1992).

37. M. NAKAGAWA and T. MORI, "MORSE-DD; A Monte Carlo Code Using Multi-Group Double Differential Form Cross Section," JAERI-M 84-126, Japan Atomic Energy Research Institute (1984).

38. K. MAKI et al., "Nuclear Group Constant Set FUSION-J3 for Fusion Reactor Nuclear Calculations Based on JENDL-3," JAERI-M 91-072, Japan Atomic Energy Research Institute (1991).

39. K. SHIBATA et al., "Japanese Evaluated Nuclear Data Library, Version-3," JAERI-1319, Japan Atomic Energy Research Institute (1990).

40. Y. IKEDA et al., "Joint Report of JAERI/USDOE Collaborative Program on Fusion Neutronics—Induced Radioactivity Measurements in Fusion Neutron Environment," JAERI-M 93-018, UCLA-ENG-91-32, UCLA-FTN-53, Japan Atomic Energy Research Institute (1993).

41. A. KUMAR et al., "Direct Nuclear Heating Measurements and Analyses for Plasma-Facing Materials," *Fusion Technol.*, **28**, 173 (1995).

42. M. NAKAZAWA, K. KOBAYASHI, S. IWASAKI, T. IGUCHI, K. SAKURAI, Y. IKEDA, and T. NAKAGAWA, "JENDL Dosimetry File," JAERI-1325, Japan Atomic Energy Research Institute (1992).

43. Y. IKEDA, C. KONNO, Y. OYAMA, K. KOSAKO, K. OISHI, and H. MAEKAWA, "Absolute Measurements of Activation Cross Sections of 27Al(n,p)27Mg, 27Al(n,a)24Na, 56Fe(n,p)56Mn, 90Zr(n,2n)89m+gZr and 93Nb(n,2n)92mNb at an Energy Range from 13.3 to 14.9 MeV," *J. Nucl. Sci. Technol.* (to be published).

44. Y. IKEDA et al., "Activation Cross Section Measurements for Fusion Reactor Structural Materials at Neutron Energy from 13.3 to 15.0 MeV Using FNS Facility," JAERI-1312, Japan Atomic Energy Research Institute (1988).

45. M. NAKAGAWA, T. MORI, K. KOSAKO, Y. OYAMA, and T. NAKAMURA, "JAERI/U.S.Collaborative Program on Fusion Blanket Neutronics—Analysis of Phase-IIA and IIB Experiments," JAERI-M 89-154, Japan Atomic Energy Research Institute (1989).

Yujiro Ikeda (PhD, nuclear engineering, Nagoya University, Japan, 1981) is head of the Fusion Neutronics Laboratory in the Department of Reactor Engineering at the Japan Atomic Energy Research Institute (JAERI). He has worked in the areas of fusion neutronics experiments, induced radioactivity

experiment and analysis, direct nuclear heating measurements, activation cross-section measurements, and fusion dosimetry.

Anil Kumar (PhD, University of Bombay, India, 1981) is senior development engineer at the University of California, Los Angeles (UCLA). His current research interests include fusion reactor nucleonics experiments and analysis, technique development for nuclear heating, decay heat measurements, biological dose, fusion diagnostics, safety factor methodology for fusion reactor design parameters, low-activation materials, inertial confinement fusion, and sequential reactions. He has conducted experiments at leading facilities such as the Fusion Neutronics Source (FNS) facility in Japan, the Tokamak Fusion Test Reactor (TFTR) at Princeton University, and LOTUS in Switzerland.

Chikara Konno (MS, physics, Kyoto University, Japan, 1985) is a research scientist in the Department of Reactor Engineering at JAERI. He has worked in the areas of fusion neutronics experiments, cross-section measurements, and neutron spectrum measurements using a proton-recoil counter.

Kazuaki Kosako (BE, atomic engineering, Tokai University, Japan, 1984) has worked at Sumitomo Atomic Energy Industries since 1994. He worked in the Department of Reactor Engineering at JAERI from 1984 to 1992 where he was involved mainly in fusion neutronics. He is currently interested in the area of radiation damage of materials.

Yukio Oyama (BS, physics, 1975; MS, nuclear physics, 1977; and Dr. Eng., 1989, Osaka University, Japan) is a principal scientist at JAERI. He has worked in the area of fusion neutronics experiments since 1978. He is currently involved in intense and high-energy neutron source projects.

Fujio Maekawa (MS, nuclear engineering, Osaka University, Japan, 1990) is a research scientist at JAERI. He has been engaged in integral experiments for fusion neutronics and studied the behavior of neutron, photon, and electron transport in media. His current interests are in the measurements of tritium and decay heat of irradiated materials.

Hiroshi Maekawa (BE, 1965; MS, 1967; and Dr. Eng., 1970, nuclear engineering, Tokyo Institute of Technology, Japan) is the deputy director of the Department of Reactor Engineering and the head of the Intense Neutron Source Laboratory at JAERI. He has worked on fusion neutronics for more than 20 years, and he planned and constructed the FNS facility. He served as the Japanese leader of the JAERI/U.S. Department of Energy (U.S. DOE) collaboration on fusion blanket neutronics. His recent research has focused on International Fusion Materials Irradiation Facility conceptual design activities.

Mahmoud Z. Youssef (PhD, nuclear engineering, University of Wisconsin, 1980) is a senior research engineer in the Department of Mechanical, Aerospace, and Nuclear Engineering at UCLA. He participated in several conceptual magnetic fusion energy and inertial fusion energy reactor design studies with emphasis on nuclear analysis and blanket/shield design. His research interests are in the areas of blanket/shield design optimization, nuclear data, sensitivity/uncertainty studies, neutronics methods and code development, tritium fuel cycle, radioactivity and safety aspects of fusion, integral experiments, neutronics testing, and research and development for fusion reactors, particularly the International Thermonuclear Experimental Reactor (ITER).

Mohamed A. Abdou is a professor in the Department of Mechanical, Aerospace, and Nuclear Engineering at UCLA and also is the director of fusion technology at UCLA. His research interests include neutronics, thermomechanics, fusion technology, and reactor design and analysis. He served as the U.S. leader of the JAERI/U.S. DOE collaboration on fusion blanket neutronics.